HHS Public Access

Author manuscript

Curr Biol. Author manuscript; available in PMC 2025 January 22.

Published in final edited form as:

Curr Biol. 2024 January 22; 34(2): 389–402.e5. doi:10.1016/j.cub.2023.12.046.

Hypothalamic CRF neurons facilitate brain reward function

Xinli Xu[1,#], **Shuidiao Zheng**[1,4,#], **Jiayan Ren**[1,#], **Zixuan Li**[1,3,#], **Jinyan Li**[1], **Zhibin Xu**[2], **Feng Yuan**[1], **Qixing Yang**[1], **Alexander V. Margetts**[5], **Tate A. Pollock**[5], **Samara J. Vilca**[5], **Canyu Yang**[7], **Gaowei Chen**[1], **Peilei Shen**[2], **Shupeng Li**[7], **JianXun Xia**[8], **Chuyun Chen**[4], **Tao Zhou**[1,3], **Yingjie Zhu**[1,3], **Luis M. Tuesta**[5], **Liping Wang**[2,3], **Paul J. Kenny**[6], **Xin-an Liu**[2,3,*], **Zuxin Chen**[1,3,9,*]

[1]Shenzhen Key Laboratory of Drug Addiction, Shenzhen Neher Neural Plasticity Laboratory, the Brain Cognition and Brain Disease Institute, Shenzhen Institute of Advanced Technology, Chinese Academy of Sciences (CAS); Shenzhen-Hong Kong Institute of Brain Science-Shenzhen Fundamental Research Institutions, Shenzhen, 518055, China

[2]Guangdong Provincial Key Laboratory of Brain Connectome and Behavior, CAS Key Laboratory of Brain Connectome and Manipulation, Brain Cognition and Brain Disease Institute (BCBDI), Shenzhen Institute of Advanced Technology, Chinese Academy of Sciences, Shenzhen-Hong Kong Institute of Brain Science-Shenzhen Fundamental Research Institutions, Shenzhen, 518055, China

[3]University of Chinese Academy of Sciences, Beijing, 100049, China

[4]The Affiliated Traditional Chinese Medicine Hospital of Guangzhou Medical University, Guangzhou, Guangdong 510130, China

[5]Department of Psychiatry and Behavioral Sciences, University of Miami Miller School of Medicine, Miami, FL 33136, USA

[6]Nash Family Department of Neuroscience, Icahn School of Medicine at Mount Sinai, New York, NY 10029, USA

[7]State Key Laboratory of Oncogenomics, School of Chemical Biology and Biotechnology, Peking University Shenzhen Graduate School, Shenzhen, China

[8]Yunkang School of Medicine and Health, Nanfang College, Guangzhou, Guangdong, 510970, China

[9]Lead contact

[*]**Corresponding authors:** Xin-an Liu; Zuxin Chen. xa.liu@siat.ac.cn ; zx.chen3@siat.ac.cn.
[#]These authors contributed equally.

Author Contributions

X.X, L.M.T, P.J.K, X.L, Z.C designed research; X.X, S.Z, J.R, Z.L, Z.X, J.L, F.F, Q.Y, C.Y, A.V.M, T.A.P, S.J.V and X.J.X performed research; G.C, P.S, C.C, T.Z, L.W, Y.Z and S.L contributed new reagents/analytical tools; X.X, S.Z, J.R, Z.L, L.M., X.L and Z.C analyzed data; X.X, P.J.K, X.L and Z.C wrote the paper.

DECLARATION OF INTERESTS

The authors declare no competing interests.

Summary

Aversive stimuli activate corticotropin-releasing factor (CRF)-expressing neurons in the paraventricular nucleus of hypothalamus (PVN^{CRF} neurons) and other brain stress systems to facilitate avoidance behaviors. Appetitive stimuli also engage the brain stress systems, but their contributions to reward-related behaviors are less well understood. Here, we show that mice work vigorously to optically activate PVN^{CRF} neurons in an operant chamber, indicating a reinforcing nature of these neurons. The reinforcing property of these neurons is not mediated by activation of the hypothalamic-pituitary-adrenal (HPA) axis. We found that PVN^{CRF} neurons send direct projections to the ventral tegmental area (VTA), and selective activation of these projections induced robust self-stimulation behaviors, without activation of the HPA axis. Similar to the PVN^{CRF} cell bodies, self-stimulation of PVN^{CRF}-VTA projection was dramatically attenuated by systemic pretreatment of CRF receptor 1 or D1 dopamine receptor (D1R) antagonist, and augmented by corticosterone synthesis inhibitor metyrapone, but not altered by D2 dopamine receptor (D2R) antagonist. Furthermore, we found that activation of PVN^{CRF}-VTA projections increased c-Fos expression in the VTA dopamine neurons, and rapidly triggered dopamine release in the nucleus accumbens (NAc), and microinfusion of D1R or D2R antagonist into the NAc decreased the self-stimulation of these projections. Together, our findings reveal an unappreciated role of PVN^{CRF} neurons and their VTA projections in driving reward-related behaviors, independent of their core neuroendocrine functions. As activation of PVN^{CRF} neurons is the final common path for many stress systems, our study suggests a novel mechanism underlying the positive reinforcing effect of stressful stimuli.

eTOC Blurb:

Xu et al. uncover an unappreciated role of PVN^{CRF} neurons in promoting reward-related behaviors through a mechanism involving activation of the PVN^{CRF}-VTA-NAc circuitry, independent of their role in regulation of the HPA axis. This study may reveal an important neuronal circuitry underlying the positive reinforcing effect of stressful stimuli.

Introduction

Aversive stimuli engage stress systems in the brain, which promotes avoidance behaviors [1,2]. However, not all stressful stimuli are aversive and promote avoidance. Certain individuals actively seek stressful situations; for instance, engaging in high-risk sports such as rock climbing [3,4]. This behavior has also been noted in rodents, such as rats that show a greater willingness to explore potentially threatening and stress-evoking novel environments [5,6]. Acute stress facilitates mesolimbic dopamine transmission [7–9], which may contribute to the reinforcing properties of some stressful stimuli. However, the neuronal substrates mediating the positive reinforcing effect of stress are largely unknown.

Corticotropin-releasing factor (CRF) is a neuropeptide released by populations of neurons in the brain during exposure to stressful stimuli [10–12]. Aversive stimuli that promote avoidance behaviors are known to activate CRF-expressing neurons throughout the brain [13]. However, emerging evidences suggest that of CRF systems can also promote appetitive behaviors [14–16]. Activation of CRF neurons in the paraventricular nucleus of hypothalamus

(PVN) is a final common path for many stress systems in the brain that engage the hypothalamic-pituitary-adrenal (HPA) axis to release glucocorticoids from the adrenal gland [2,17]. Interestingly, rats will volitionally self-administer corticosterone (the major glucocorticoid in rodents), suggesting that stress-related glucocorticoids can have positive rewarding properties [18]. Recent studies found that CRF neurons in the PVN (PVN^{CRF} neurons) were rapidly activated by aversive stimuli, and repeated activation of these neurons induced avoidance behavior in mice [12,19]. This led to the suggestion that activation of PVN^{CRF} neurons encoded stress-related aversive behavioral states [12,19]. However, it was found that mice subjected to mild stress had improved health outcome through PVN^{CRF} neurons activation mechanisms [20,21]. Thus, activation of PVN^{CRF} neurons could potentially mediate the motivational effects of stress in a dynamic manner, depends on the forms and strength of the stimuli. Interestingly, it was found that activation of CRF signaling could enhance the activity of the dopamine neurons in the ventral tegmental area (VTA) and thus probably involved in the pursuit of appetitive behaviors [22,23]. However, whether activation of PVN^{CRF} neurons can drive appetitive behavior, and how they affect the activity of the midbrain dopamine neurons and the release of dopamine in the mesolimbic system are still unknown.

Here in this study, we aimed to address the following questions: 1) Does acute activation of PVN^{CRF} neurons have positive reinforcing properties. 2) If so, are these reinforcing properties dependent on the activation of HPA axis? 3) What is the role of the mesolimbic dopamine system in their reinforcing properties? To answer these questions, we tested whether activation of PVN^{CRF} neurons supports operant self-stimulation behavior in mice, an approach adapted from classical intracranial electrical self-stimulation procedures that can be used to access the reinforcing properties of genetically defined populations of neurons in the brain and the brain regions to which they project [24]. By combining behavioral, histochemical, pharmacological analyses along with the *in vivo* dopamine imaging techniques, we found that activation of PVN^{CRF} neurons facilitate reward behaviors through a mechanism involving enhanced VTA-derived dopamine release in NAc but independent of HPA axis stress hormones. Thus, our study may have identified a key neural substrate underlying the positive reinforcing effect of stressful stimuli.

Results

Optical activation of PVN^{CRF} neurons supports self-stimulation behavior

To activate PVN^{CRF} neurons, we injected an adeno-associated virus to express the light-activated ion channel channelrhodopsin-2 in a Cre-dependent manner (AAV-DIO-ChR2-mCherry) or a control virus (AAV-DIO-mCherry) into the PVN of the CRF-Cre mice (Jax 012704), a transgenic line that has been widely used for specific manipulation of PVN^{CRF} neurons [12,19,25–28]. The injected mice were referred as PVN^{CRF}-ChR2 and PVN^{CRF}-mCherry mice in this study, respectively. In brain slices, we verified that blue light deliveries induced firing of action potentials in the PVN^{CRF}-ChR2 neurons at frequencies up to 20Hz (Figure S1). To control CRF neurons *in vivo,* an optical fiber was implanted above the PVN for light stimulation in these injected mice (Figures 1A and B). We found that blue light delivery (473 nm, 10 Hz) induced robust grooming behavior (Video S1)

and increased plasma corticosterone (CORT) levels in the PVN^{CRF}-ChR2 mice but not in the control mice (Figures 1C and 1D). Increased grooming time and circulating CORT levels are typical hallmarks of activation of PVN^{CRF} neurons as demonstrated by previous findings [12,27]. Next, we investigated whether acute activation of PVN^{CRF} neurons modified reward-related behaviors. We began by testing the mice in a real-time place preference/avoidance (RTPP/A) paradigm using an apparatus with two interconnected chambers (Figure 1E). Mice were tested during 15 min sessions on 2 consecutive days. On day 1, they were permitted to freely explore both chambers of the apparatus to assess baseline preference for either chamber in the absence of optical stimulation. On day 2, each entrance into one side of the chamber (counterbalanced across animals) triggered the activation of a laser that delivered 10 Hz continuous optical stimulation until the mouse exited the chamber. The animals were allowed to freely move between chambers during the test. Thus, if optical stimulation of PVN^{CRF} neurons has reward or aversion related effects, the mice would be expected to spend more or less time, respectively, in the laser-paired chamber. We found the average time spent in the laser paired-chamber was not significant different between the baseline day and RTPP/A test day in either ChR2 group or the control group (Figures 1F and 1G). However, closer inspection of the data revealed strikingly different patterns of behavior in the ChR2 group, with 30% of the mice showing robust avoidance behavior, and 40% showing robust preference behavior (Figure 1G). It was found that, in some instance, mice would frequently enter and exit the stimulation-paired chamber for brief stimulation to maximize the reinforcing effect during RTPP/A test [29]. Thus, we also analyzed the number of entries into the laser-paired chamber during baseline and the RTPP/A test for the PVN^{CRF}-ChR2 mice. We found that the average number of entries into the stimulation-paired chamber for these mice was not significantly changed in the test day (Figure S2). The subset of mice which spent less time in the stimulation-paired chamber (with negative preference score) did not show an increase of entries into the chamber during the test (Paired t test, p=0.9, n=5 mice) (Figure S2). In fact, most of the PVN^{CRF}-ChR2 mice showed a decreased number of entries into the laser paired-chamber during the RTPP/A test (Figure S2). Based on these observations, we speculated that non-volitional stimulation of PVN^{CRF} neurons was rewarding in some ChR2 nice but aversive in others. Therefore, we permitted the mice to control the optical activation of PVN^{CRF} neuron using a volitional self-stimulation procedure. Specifically, mice were given the opportunity to respond freely at two identical nosepoke ports in operant chambers. A nosepoke at the active port resulted in 1–20 Hz optical stimulation for 1s duration (Figure 1H). We found that ChR2 mice permitted to respond for higher frequency optical stimulation (10–20 Hz) and demonstrated vigorous self-stimulation behavior (Figures 1I, S3, and Video S2). By contrast, ChR2 mice failed to reliably respond for lower frequency (2 Hz) optical stimulation (Figure S3). The mCherry-expressing control mice failed to reliably respond for optical stimulation (10Hz) (Figure 1J). Number of self-stimulation responses in ChR2 mice were uncorrelated to their behavior in the RTPP/A test (Figure 1K). Together, these findings suggest that volitional activation of PVN^{CRF} neurons has positive reinforcing properties.

PVN^{CRF} projections to VTA promote reward-related behaviors

Next, we sought to define the circuit-based mechanisms by which PVN^{CRF} neurons elicit reward-related behaviors. Given that dopamine neurons in ventral midbrain play

well-established roles in appetitive behaviors [30,31], we asked whether the VTA was the downstream target of PVN^{CRF} neurons in mediating the reward-related behavior. First, immunofluorescence staining from the PVN^{CRF}-ChR2 mice revelated intense mCherry-positive fibers in the VTA, which coincided the location of tyrosine hydroxylase (TH)-positive dopamine neurons (Figure S4), suggesting a direct projection to these neurons. Next, we investigated whether these projections support self-stimulation behavior. To this end, AAV-DIO-ChR2-mCherry was injected into the PVN of CRF-Cre mice (referred as PVN^{CRF}-VTA-ChR2 mice), with AAV-DIO-mCherry again used as a control (referred as PVN^{CRF}-VTA-mCherry mice) (Figure 2A). Optical fibers were implanted above the VTA of these mice (Figures 2A and 2B). As expected, robust ChR2-mCherry-labeled fibers were detected in the VTA of these mice (Figure 2B). Optical stimulation (20Hz) of VTA did not induce grooming behavior or alter plasma CORT levels in the PVN^{CRF}-VTA-ChR2 mice or in control mice (Figures 2C and 2D). This suggests that activation of the PVN^{CRF}-VTA circuit is unlikely to recruit the HPA axis. Mice were then tested in the RTPP/A assay according to the same procedure described above (Figure 2E). Optical stimulation delivered to the VTA induced robust preference for the stimulation-paired chamber in PVN^{CRF}-VTA-ChR2 mice but not in control mice (Figures 2F and 2G). Mice were then permitted to volitionally delivered optical stimulation to the VTA using the same self-stimulation procedure described above (Figure 2H). The PVN^{CRF}-VTA-ChR2 mice engaged in vigorous self-stimulation behavior when relatively high optical frequency stimulation was available (20–40 Hz) (Figure S5). Lower frequency stimulation parameters (10 Hz) failed to support robust self-stimulation behavior (Figure S5).We then performed the operant self-stimulation experiment on PVN^{CRF}-VTA-ChR2 mice that had received RTPP/A test previously. We found that all of these mice showed robust and stable self-stimulation behaviors over consecutive daily sessions (Figure 2I and Video S3). The average number of active port responses from all of the PVN^{CRF}-VTA-ChR2 mice we have tested in this study was 909, much higher than their inactive port responses with an average number of 8 (Figure 2J). By contrast, the average number of active port and inactive responses from the control mice was 5 and 6, respectively (Figure 2K). Taken together, these data demonstrate that the PVN^{CRF}-VTA circuit supports reward-related behaviors independent of the HPA axis.

PVN^{CRF} neurons promote reward-related behaviors independently of HPA axis activation

Activation of PVN^{CRF} neurons by stress is known to drive the HPA axis by triggering the release of adrenocorticotropic hormone (ACTH) into the blood stream from the pituitary, then the circulating ACTH subsequently acts in the adrenal cortex to induce the secretion of CORT, which exerts multiple functions by binding to its receptors in the brain or in the peripheral organs[32]. Interestingly, it was found that CORT (the end product of HPA axis) has positive reinforcing effects in rodents [18]. Thus, we wanted to know whether HPA axis also plays a role in the reinforcing property of PVN CRF neurons. To this end, we investigated whether pharmacological manipulation of the HPA axis alters the self-stimulation behaviors in the PVN^{CRF}-ChR2 mice. We found that systemic injection of CORT, or the ACTH receptors antagonist $ACTH_{(11–24)}$ (for blockage of the ACTH signaling), or the glucocorticoid receptor antagonist RU38486 (for blockage of the CORT signaling) did not significantly change the operant self-stimulation behaviors in these mice (Figures 3A–3C and 3I). These results together support that the reinforcing effects of

PVN^{CRF} neurons are not mediated by their role in activation of the neuroendocrine HPA axis.

PVN^{CRF} neurons and their projections to VTA act through CRF and dopamine transmission to promote reward-related behaviors

Our findings suggested the reinforcing effects of PVN^{CRF} neurons are probably mediated by their projection to VTA. Next, we used the pharmacological approaches to further confirm this hypothesis. Previous study found that CRF application enhanced the firing rate of VTA dopaminergic neurons by directly acting on CRF1 receptor (CRFR1) but not on CRF2 receptor (CRFR2) [22]. Thus, we tested whether the self-stimulation behaviors were dependent on the activation of CRFR1. We found that systemic injection of the CRF1 receptor (CRFR1) antagonist antalarmin attenuated the self-stimulation behaviors in both PVN^{CRF}-ChR2 and PVN^{CRF}-VTA-ChR2 mice (Figures 3D, 3I, 3J and 3P). Furthermore, systemic injection of the dopamine 1 receptor (D1R) antagonist SCH23390 also attenuated the self-stimulation behaviors in both PVN^{CRF}-ChR2 and PVN^{CRF}-VTA-ChR2 mice, whereas a dopamine 2 receptor (D2R) antagonist eticlopride had no effect (Figures 3E, 3F, 3I, 3K, 3L, and 3P). A combination of SCH23390 and eticlopride did not result in a further suppression of the self-stimulation behaviors in the PVN^{CRF}-VTA-ChR2 mice, when compared with SCH23390 alone (Figures 3M and 3P). Interestingly, self-stimulation behaviors in PVN^{CRF}-ChR2 and PVN^{CRF}-VTA-ChR2 mice were both enhanced after pretreatment with the glucocorticoid synthesis inhibitor metyrapone (Figures 3G, 3I, 3N, and 3P). Metyrapone is known to upregulate CRF levels and enhance the intrinsic excitability of PVN CRF neurons due to the suppression of CORT-negative feedback [26,33], which likely explains the enhanced self-stimulation behaviors that we observed. Consistent with this interpretation, physical stressors known to increase CRF activity in the brain such as tail suspension stress[12] also enhanced self-stimulation behaviors in PVN^{CRF}-VTA-ChR2 mice (Figures 3O and 3P). Finally, as oxytocin-producing neurons in the PVN have been reported to promote social rewards [34], we tested whether oxytocin contributes to the reinforcing effects of PVN^{CRF} neurons. Systemic pretreatment with the oxytocin receptor antagonist L-368,899 did not affect the self-stimulation behaviors in the PVN^{CRF}-ChR2 mice (Figures 3H and 3I). Taken together, these results suggest that CRF released by PVN^{CRF} neurons acts in the CRFR1 expressing dopamine neurons in VTA to enhance dopamine neurotransmission, which promotes reward-related behaviors. Moreover, given the similar effects of the blockers were found in both the PVN^{CRF}-ChR2 and PVN^{CRF}-VTA-ChR2 mice, these results further support the idea that the reinforcing effects of PVN^{CRF} neurons are mediated by their projections to the VTA.

Operant self-stimulation behaviors driven by activation of VTA neurons in C57BL/6J mice

Our findings demonstrated a specific dopamine receptor signaling underlying the reinforcing effects of PVN CRF neurons and the PVN^{CRF}-VTA neural circuitry. We next investigated whether this specificity is unique with PVN CRF-dopaminergic neurons interaction in the VTA, or it is a general effect of stimulating VTA neurons. To this end, we induced ChR2 expression in VTA neurons by unilaterally injecting AAV-hSyn-ChR2-mCherry into the VTA region of C57BL/6J mice (referred as C57BL/6J-VTA-ChR2 mice), and implanted an optical fiber above the VTA assaying self-stimulation behaviors (Figure 4A). VTA

neuronal activation promoted self-stimulation behaviors in these mice, whereas a much smaller number of active nose pokes was achieved than that observed in PVN^{CRF}-VTA-ChR2 mice under similar conditions (Figure 4B). Pharmacological analyses revealed that the self-stimulation behaviors of these mice were attenuated by pretreatment with D1R or D2R antagonists alone or with the combination of these antagonists (Figures 4C–4E and 4I). Our finding was in line with previous study showing that local antagonism of either D1R or D2R in NAc attenuated the positive reinforcement effects of VTA dopaminergic neurons[31,35]. Furthermore, pretreatment with metyrapone significantly decreased self-stimulation behaviors in these mice (Figures 4F and 4I), which was opposite to the results obtained via the stimulation of PVN^{CRF} neurons or their terminals in the VTA. Prior acute restraint stress significantly decreased the self-stimulation behaviors in these mice, whereas acute tail suspension showed no significant effects (Figures 4G–4I). Taken together, these findings suggest that the reinforcing property of PVN^{CRF} neurons is mediated by activation of a unique subpopulation of VTA neurons.

$PVN^{CRF}\rightarrow$ VTA projections increase neural activity of dopamine neurons in the VTA

Next, we thought to confirm the dopamine neurons in VTA mediate the rewarding effect of PVN^{CRF} projections. To this end, we conducted immunostaining of c-Fos (an indicator of neuronal activation) in the VTA-containing brain slices from control and PVN^{CRF}-VTA-ChR2 mice that were permitted to perform optical self-stimulation behavior for 90 min (Figure 5A). We detected increased numbers of c-Fos-positive cells, especially in TH-expressing neurons in the VTA of PVN^{CRF}-VTA-ChR2 mice relative to control mice (Figures 5B–5D). As it was found that CRF activated dopamine neuron via directly acting on CRFR1 but not CRFR2 [22], together with our findings that self-stimulation behaviors of PVN^{CRF} neurons and their projections to VTA were attenuated by CRFR1 antagonist antalarmin, we speculated that CRFR1 may be the primary receptor in the dopamine neurons. Thus, we performed cell type-specific nuclear RNA sequencing with the midbrain tissue of mice using a similar approach as previously described [36]. We observed that *Crfr1* but not *Crfr2* gene transcripts were abundantly expressed by midbrain dopaminergic neurons (Figure S6). These data together suggest that PVN^{CRF} projections are likely to enhance the activity of VTA dopaminergic neurons via CRF1 receptors.

$PVN^{CRF}\rightarrow$VTA projections stimulate dopamine transmission in the NAc

The NAc is a major projection target of VTA dopaminergic neurons, and the release of dopamine into this area supports self-stimulation behaviors in rodents [35,37]. Thus, we used in vivo photometry recording combined with a genetically encoded dopamine sensor sensors[38] to investigate whether $PVN^{CRF}\rightarrow$VTA projections stimulate dopamine transmission in the NAc. AAV-DIO-ChR2-mCherry virus was injected into the PVN of CRF-Cre mice and optical fibers were implanted above the VTA for stimulation. In addition, AAV-hSyn-DA4.4 virus was injected in the NAc of the same animal to express the dopamine sensor $GRAB_{DA2m}$ and an optical fiber was implanted above NAc for *in vivo* photometric recording of dopamine signals (Figure 5E). This preparation permitted us to stimulate $PVN^{CRF}\rightarrow$VTA projections while concurrently monitoring dopamine signaling in the NAc. We confirmed the expression of $GRAB_{DA2m}$ sensor was restricted to the NAc (Figure 5F). Moreover, we found that activation of $PVN^{CRF}\rightarrow$VTA projections induced a rapid

and robust dopamine-related response from the $GRAB_{DA2m}$ sensor relative to baseline fluorescence levels (Figures 5G–5 I). Thus, these results demonstrated that activation of PVN^{CRF} terminals enhanced VTA-derived dopamine neurotransmission in the NAc. Furthermore, these results are in line with the observation of increased c-Fos positive cells in the VTA dopamine neurons after stimulation of the PVN^{CRF}→ VTA projections.

The self-stimulation behaviors of PVN^{CRF}→VTA projections require both D1R and D2R activation in the NAc

Our results suggested that the reinforcing property of PVN^{CRF}→VTA projection probably mediated by enhancing dopamine release in the NAc. If so, blockage of dopamine neurotransmission in the NAc should attenuate the self-stimulation behaviors driven by the activation of the PVN^{CRF}→VTA projection. To test this idea, we implanted cannulas into the NAc of the PVN^{CRF}-VTA-ChR2 mice and investigated how intra-NAc infusion of dopamine receptors antagonists affected their operant self-stimulation behaviors (Figure 6A). We found that intra-NAc infusion of D1R antagonist SCH23390 or D2R antagonist eticlopride significantly decreased the self-stimulation behaviors in these mice (Figures 6B–6D). Thus, these results further confirmed that the reinforcing property of PVN^{CRF}→VTA projection was mediated by dopamine transmission in the NAc, and dependent on the activation of both D1R and D2R.

Discussion

In the present study, we have revealed an unappreciated role of PVN^{CRF} neurons in promotive reward-related behaviors through a mechanism involving enhanced VTA-derived dopamine neurotransmission but independent of HPA axis stress hormones. Given the important roles of PVN^{CRF} neurons in coordinating physiological and behavioral responses to acute stressors, our study has uncovered a potential neural substrate underlying the appetitive qualities of stressful stimuli, and expanded the current understanding of the roles of these neurons in adaptive coping behaviors of stressful stimuli, independent of their core neuroendocrine functions [14–16,18].

In our study, we aimed to understand how acute activation of the PVN CRF neurons affects reward-related behaviors. We began by testing the PVN^{CRF}-ChR2 mice with the RTPP/A assay. The tests were conducted in a 2-day schedule, with the first day to determine the baseline preference of the mice and the second day to test their preference to the stimulation-paired chamber. Our data showed that acute activation of the PVN CRF neurons did not induce overall significant preference or avoidance during the test day. A previous study has tested whether activation of the PVN CRF neurons could serve as an unconditioned stimulus for the formation of aversive memories[12]. Their tests were performed in a 6-day schedule, with the first day to determine the baseline preference of the mice, followed with a 4 day-conditioning in the RTPP/A assay, and tested the post-conditioning effect on day 6 without stimulation. They also found that acute activation of PVN CRF neurons did not induce significant preference or avoidance during the first day of RTPP/A test, which is consistent with our observation[12]. Interestingly, the mice started to show a significant avoidance to the stimulation-paired chamber at day 5, which was after 3 days of stimulation conditioning[12].

These findings, together with our current results, suggest that repeated activation, but not acute activation, of the PVN CRF neurons, induces conditioned avoidance behavior and aversion memory formation in the mice.

Our study found that a subset of PVN^{CRF}-ChR2 mice showed strong avoidance (less time, less entries) in the stimulation-paired chamber during the RTPP/A but these mice also had robust operant responding for self-stimulation seems paradoxical (Figure 1K). Although place conditioning and operant conditioning have been widely used in in parallel to assess motivational behaviors, but studies showed that they have apparent discrepancies such as conditioning cues and volitional control by the tested animal[39]. In a typical RTPP/A assay, mice receive optical stimulation once they enter the stimulation paired-chamber and the stimulation continues until they exit. The longer the time spent in the stimulation paired-chamber suggests a stronger reinforcing effects, or vise versa. Interestingly, it was found that mice would frequently enter and exit the stimulation paired-chamber for brief stimulation to maximize the reinforcing effect and to avoid the aversion after long period of stimulation[29]. Whereas in the operant self-stimulation assay, each nose poke of the mice resulted in a short and fixed duration of stimulation, the mice would have better control of the stimulation (volitional) to avoid aversion effects induced by overstimulation. Given that operant self-stimulation behaviors were found in all of the PVN^{CRF}-ChR2 mice, including those that exhibited significant avoidance during the RTPP/A test, together with the finding that repeated stimulation of the PVN CRF neurons induced conditional place avoidance[12], further supports the notion that overstimulation of these neurons induces aversive rather than rewarding effects. Thus, the valence of PVN CRF neurons depends on the intensity and duration of the stimulation. The paradoxical preference shown by PVN^{CRF}-ChR2 mice in the RTPP/A test (some mice showed preference while others showed avoidance) may be due to different degrees of excitation of PVN CRF neurons triggered by blue light. Factors contributing to different sensitivities to light stimulation between animals may include the total number of CRF cells expressed ChR2, the expression levels of ChR2, and the locations of the optical fiber tips, etc. The rewarding effects of PVN CRF neurons are most likely mediated by their projections to the VTA, as stimulation of these projections induces significant real time place preference and also supports robust operant self-stimulation behaviors. The downstream brain areas mediating the aversive effects of PVN CRF neurons may include the lateral hypothalamus or globus pallidus (GPe) [17,40]. Together, our findings suggest that activation of PVN CRF neurons may convey both rewarding and avoidance information, depending on the intensity, novelty, durations and controllability of the stimuli.

VTA CRF signaling has been implicated in stress-induced impairments of motivational behaviors [41–44]. Previous studies have demonstrated a complex interaction between CRF and dopamine systems in the VTA. For instance, it was found that CRF perfusion could increase firing rates of dopamine neurons in *ex vivo* brain slices[22,44]; but, in vivo study found that local infusion of exogenous CRF into VTA decreased dopamine release in NAc [41]. These inconsistent findings could be attributed to the complexity of VTA neurons and the distribution of the CRF receptors [45,46]. However, the mechanisms underlying the regulation of VTA dopaminergic neurons and related motivational behaviors by endogenous CRF remain unclear. With combination of optogenetic stimulation and simultaneous *in vivo* dopamine sensor recording, we were able to detect rapid dopamine release in the NAc

while stimulating the PVN CRF terminals in the VTA. Given the fast kinetic dopamine release observed during the experiment, our data suggests that endogenous release of CRF can rapidly activate the VTA dopamine neurons that projecting to NAc. The increased DA activity by stimulation of PVN^{CRF}→VTA projections was unlikely caused by the disinhibition of VTA interneurons via CRF signaling, as it is known that activation CRF receptors are primarily signaled by excitatory Gs/Gq protein [47]. Although both CRFR1 and CRFR2 have been showed regulating the activity of VTA dopamine neurons, the CRF/CRFR1 signaling probably plays an important role in mediating the fast excitation effect in the VTA DA neurons and reward-related behavior, as evidenced by: 1) CRFR1 is the most abundant CRF receptors in VTA dopamine neurons; 2) The self-stimulation behaviors with either activation of the PVN CRF cell bodies or their terminals in VTA were attenuated by CRFR1 antagonist, and augmented by metyrapone which is known to elevate CRF levels [26]; 3) Previous study found that CRF increased the firing rate of VTA dopamine neurons via CRFR1-dependent and CRFR2-independent mechanism in brain slices [22]; 4) In contrast to the direct excitatory effect mediated by activation of CRFR1, the excitatory effect of CRFR2 on VTA dopamine neurons was found mainly mediated through the enhancement of glutamatergic synaptic transmission in these neurons, thus requiring the simultaneous stimulation of the excitatory afferent projections [48]. Moreover, the excitatory effect mediated by CRFR2 was slow and transient [48,49]; 5) CRF has a higher affinity for CRFR1 and a low affinity for CRFR2 [50]. Consistent with our findings, a recent study found that the CRFR1 expression levels in VTA dopamine neurons determined the motivational properties of acute stress [44]. Together with the observation that self-stimulation of PVN CRF terminals in the VTA was dependent on D1R and D2R in the NAc, our study suggests that PVN CRF neurons make synaptic connections with the CRFR1-expressing dopamine neurons in the VTA, which sending neuronal projections to D1R-expressing and D2R-expressing neurons in the NAc, and activation of this neural circuitry promotes reward-related behaviors (Figure 7). To the best of our knowledge, our study reveals for the first time how PVN^{CRF}→VTA projections regulate VTA neurons and their function in reward-related behaviors.

In summary, we have uncovered a role of PVN CRF neurons in driving reward-related behavior and a neuronal substrate that may underlie the positive reinforcing effect of stress, which independently of HPA axis activation. Furthermore, our findings provide the rationale for investigating the role and function of the PVN^{CRF}-VTA projections in the pathology of mental disorders such as depression and addiction, which have been linked with dysfunction of CRF and dopamine transmission [13,30,51].

Limitations of this study

Our current findings have revealed an important role of CRF/CRFR1 signaling in promoting reward-related behaviors. We have ruled out a potential role of oxytocin in this regard, however, further study is required to investigate the potential roles of other neurotransmitters/neuropeptides that may be co-released together with CRF. We have found that self-stimulation behaviors of the PVN^{CRF}-VTA-ChR2 mice were significantly attenuated by intra-NAc infusion of the D2R antagonist Eticlopride, but not altered by systemic injection of Eticlopride. These observations implicate that D2R expression in other brain regions are also involved in the rewarding effect of the PVN CRF neurons, and that

activation of D2R in these regions may counteract the effect of D2R in the NAc. Future studies are needed to determine the neuronal mechanisms for how D2R signaling in different brain areas affects the rewarding effect of the PVN CRF neurons. We have identified a PVN^{CRF}-VTA-NAc neural circuitry facilitates brain function in normal healthy mice, further study is required to study its role in the pathology of mental disorders such as anxiety, depression and drug addiction.

RESOURCE AVAILABILITY

Lead contact

Further information and requests for resources and reagents should be directed to and will be fulfilled by the lead contact, Zuxin Chen (zx.chen3@siat.ac.cn).

Material availability

This study did not generate new unique reagents.

Data and code availability

This paper does not report original code.

Analyzed data and images reported in this paper will be shared by the lead contact upon request.

Any additional information required to reanalyze the data reported in this paper is available from the lead contact upon request.

EXPERIMENTAL MODEL DETAILS

All experimental procedures involving the use of animals in this study were approved by the Institutional Animal Care and Use Committee (SIAT-IACUC-210913-NS-CZX-A2055) of the Shenzhen Institute of Advanced Technology, Chinese Academy of Sciences. Adult (8 to 24 weeks old) CRF-Cre mice (Jax No. 012704) [28] and C57BL/6J mice were used. Mice were maintained at 22–25°C on a circadian 12-h light/dark cycle with food and water available *ad libitum*.

METHOD DETAILS

AAV injection, optic fiber implantation and cannulation

AAV vectors—The adeno-associated viruses (AAVs) used in this study were as follows: AAV2/9-hEF1α-DIO-mCherry (Shanghai Taitool Bioscience Co., Ltd., China), AAV2/9-hEF1α-DIO-hChR2(H134R)-mCherry and rAAV-hSyn-hChR2(H134R)-mCherry (Shanghai Taitool Bioscience Co., Ltd. or BrainVTA Co., Ltd., China), and AAV9-hSyn-DA4.4 (Vigene Biosciences Co., Ltd., China). The titer used for AAVs injection was 2–10 × 10^{12} viral particles/mL.

Stereotaxic surgeries—Stereotaxic surgeries were performed under sodium pentobarbital (80 mg/kg, *i.p.*) anesthesia using a stereotaxic instrument (RWD Life Science

Co., Ltd., China). The AAVs (200–250 nL) were delivered with a glass pipette connected to a microsyringe pump (Nanoject III #3–000-207, DRUMNOND) unilaterally or bilaterally at an infusion rate of 60 nL/min. The pipette was withdrawn 10 min after the end of each injection. For fiber photometry and optogenetic activation experiments, optic fibers (diameter, 200 μm; numerical aperture [NA], 0.37; Inper, China) were chronically implanted 0.2–0.5 mm above the target area following injection and were secured with dental cement. Stereotaxic coordinates were as follows relative to Bregma (in mm): PVN [anteroposterior (AP), −0.60; mediolateral (ML), ± 0.20; dorsoventral (DV), −4.8)], VTA (AP, −3.20; ML, −0.30; DV, −4.20), NAc (AP, 1.10; ML, −0.80; DV, −4.60). For optogenetic activation experiments, AAV2/9-hEF1α-DIO-mCherry or AAV2/9-hEF1α-DIO-hChR2(H134R)-mCherry were unilaterally injected in the PVN of CRF-Cre mice and optic fibers were inserted just above the PVN (for stimulation of PVN CRF neurons) or VTA (for stimulation of PVN CRF neuronal terminals in the VTA). AAV2/9-hSyn-ChR2-mcherry virus was unilaterally injected in the VTA of C57BL/6J mice and optic fibers were implanted above VTA for photostimulation of VTA neurons. For dopamine imaging in the NAc upon optogenetic stimulation of PVN^{CRF} neuronal terminals in the VTA, AAV9-hSyn-DA4.4 was injected unilaterally (right hemisphere) in the NAc and AAV2/9-hEF1α-DIO-hChR2(H134R)-mCherry was injected unilaterally (right hemisphere) in the PVN of CRF-Cre mice. An optic fiber was implanted just above the injection site in the NAc, and another optic fiber was inserted just above the VTA (right hemisphere). For intra-NAc drug infusion experiment, AAV2/9-hEF1α-DIO-hChR2(H134R)-mCherry virus were unilaterally injected in the PVN of CRF-Cre mice and optic fibers were implanted just above VTA, a bilateral 26-gauge guide cannula was implanted into NAc (AP, 1.10; ML, ±0.80; DV, −4.60). Behavioral experiments were performed after at least 8 weeks of viral expression.

Optogenetic stimulation setup—Prior to behavioral sessions involving optogenetic stimulation, mice were gently restrained and attached to patch cables (Nanjing Aoguan Bioscience Co., Ltd., China) that were also linked to bilateral rotary joint (Nanjing Aoguan Bioscience Co., Ltd., China), which allowed free rotation while transmitting blue light from a 473 nm blue laser (SLOC Laser Systems). The laser output was measured and adjusted before each experiment. The pulse duration and stimulation frequency were controlled by a programmable pulse generator connected to the laser system. For optical self-stimulation test, the light stimulation parameters will be described in the following section.

Grooming test—The grooming behaviors were recorded in an observational chamber (35 × 35 × 40 cm) with a horizontal video camera. The behaviors of the test mouse were monitored for 10 min following a 5–5 min examination protocol in which blue light pulses were delivered in the 2^{nd} 5 min. For stimulation of PVN CRF neurons and their controls, blue light (473 nm, 20 Hz, 10 ms of pulse width, laser power between 7–15 mW) was delivered. For stimulation of PVN^{CRF} neuronal terminals in the VTA and their controls, blue light (473 nm, 40 Hz, 5 ms of pulse width, laser power between 7–15 mW) was delivered. The grooming behavior was identified and manually counted by frame-by-frame playback of video before and during optogenetic stimulation.

Real-time place preference/ avoidance (RTPP/A)—The custom-made RTPP apparatus consisted of two rectangular compartments (25 × 17 cm^2) with distinct visual and tactile environments, and interconnecting corridor separating them was used. Tracks of mouse movement were captured for 15 min at 30 frames/s with an overhead camera controlled by custom-developed tracking algorithms running on MATLAB (MathWorks Co. Ltd., USA). Mice were tested for 15 min for 2 consecutive days. On day 1, as Pre-test, mice were allowed to explore freely between two sides of the apparatus as a measure of their baseline preference. On day 2, as RTPP/A test, whenever the mouse entered one side of the apparatus, it trigged a laser on period until the mouse crossed back to the non-stimulated side. For PVN^{CRF}- mCherry/ChR2 mice, blue light (473 nm, 10 Hz or 20Hz, 10 ms of pulse width, laser power 7–15 mW) was delivered. For PVN^{CRF}-VTA-mCherry/ChR2 mice, blue light (473 nm, 20 Hz with 10 ms of pulse width, or 40Hz with 5 ms of pulse width, laser power 7–15 mW) was delivered.

Operant self-stimulation—The optical self-stimulation experiments were carried out in standard mouse operant conditioning chambers located inside the sound-attenuating cubicles equipped with a ventilation fan (Anlai Technology Co., Ltd., China). Each operant chamber was configured with 2 nose-poke ports. One port was assigned as the “active” port and the other as the “inactive” port. Responding in the active port resulted in delivery of a 1 s of light stimulation (473 nm, 10 or 20 Hz, 10 ms of pulse width, laser power 7–15 mW for PVN^{CRF}-mCherry/ChR2 mice; 473 nm, 20 Hz with 10 ms of pulse width, or 40 Hz with 5 ms of pulse width, laser power 7–15 mW for PVN^{CRF}-VTA-mCherry/ChR2 or C57BL/6J-VTA-ChR2 mice;) accompanied by illumination of a cue light above the port. A nose poke in the inactive port led to an identical light cue above the inactive port without activating the laser. Optical stimulation and responses in nose-poke ports were controlled and recorded using Anlai software (Anlai Technology Co., Ltd., China).

Pharmacological manipulations—In order to investigate the potential molecular mechanisms underlying the optogenetic self-stimulation, pharmacological studies were also performed. For that purpose, the mice received additional daily optogenetic self-stimulation training sessions prior to the initiation of drug injection to establish baseline response rates. Each compound test occurred for 2 consecutive days, with the 1^{st} day being the vehicle injection and the 2^{nd} day being the corresponding drug injection. For systemic injection, the doses administered, and pretreatment schedule were as follows: antalarmin (30 mg/kg, 30 min prior to testing), SCH23390 (0.05 mg/kg, 20 min prior to testing), eticlopride (0.05 mg/kg, 30 min prior to testing), corticosterone (10mg/kg, 30 min prior to testing), and metyrapone (150 mg/kg, 120 min prior to testing). The doses of each compound were selected based on pilot experiments or literature reports, to ensure that drug treatments were efficacious without producing significant sedation or locomotor inhibition. For the intra-NAc drug infusion, SCH23390 (0.5μg/side/0.25μl in saline) or eticlopride (0.5μg/side/0.25μl in saline) was infused into NAc by using a syringe pump (RWD, Shenzhen, China) at a rate of 0.2μl/min via 33 gauge infusers. Infusers were left in place for an additional 3 mins to allow for drug diffusion. 30mins after the infusions, the mice were placed in the operant chambers for accessing their self-stimulation behaviors. The doses of the drugs were chosen based on previous studies, which have consistently shown that microinfusion of the dugs into the NAc

of rodents do not affect their locomotion [35,52–54]. After each drug testing, mice received 2–4 additional days of re-stabilization on optogenetic self-stimulation sessions to re-establish the baseline responding level.

Corticosterone (CORT) measurement—For measuring the CORT levels, baseline blood samples were collected from the facial vein 3 days before light stimulation. A second sample was collected 15 min after the onset of light stimulation during which blue light was delivered for 5 min. The time was chosen based on a previous study, which shows optogenetic activation of PVN CRF neurons elevates CORT levels [27]. Identical light delivery protocol was applied as for grooming test. Plasma CORT levels were determined using an ELISA kit (Abcam) according to the manufacturer's instructions. The CORT level changes for each animal were calculated by subtracting baseline values from the corresponding samples obtained upon optogenetic stimulation.

$DA_{4.4}$ fluorescence signals photometry recording—Mice were connected to fiber photometry and optogenetic patch cords and placed in restraint tube to restrict activity. Mice habituated for 10 min to the restraint condition prior to data acquisition. Fluorescence signals from the genetically encoded indicator (dopamine sensor $DA_{4.4}$) in the NAc were recorded using a Fiber Photometry system (Qianao xingke, Nanjing, China) equipped with a 470 nm excitation laser to measure dopamine release [38]. Optogenetic stimulation of the PVN^{CRF} terminals in the VTA (473 nm, 40 Hz, 5 ms of pulse width, 2 s duration, laser power 10 mW) was delivered through the fiber implanted in the VTA, with a 30 s in between stimulation trials. A total of 40 stimulation trials were performed for each animal, with the first 20 trials as the sham stimulation during which the laser was off, and the last 20 trials as the experimental stimulation during which the laser was on. Fluorescence signals were sampled at 50 Hz and normalized to baseline signals to determine $\Delta F/F$, where $\Delta F/F = (F-F0)/F0$ and F0 is the mean value of the integral of the prestimulus signal (2 s).

Histology and Immunohistochemistry—Sections containing the VTA were processed for mCherry and TH double immunostaining. For the immunostaining, sections were permeabilized and blocked with 0.3% Triton-PBS containing 10% normal donkey serum (NDS) (blocking solution) for 2 hours at RT. Following blocking, sections were incubated with primary antibodies prepared in blocking solution overnight at 4°C. Sections were then washed with PBS, incubated with respective secondary antibodies for 2 hours and coverslipped with Vectashield® mounting medium containing DAPI nuclear counterstain (Vector Labs). Sources and dilutions of primary antibodies were as follows: rabbit anti-mCherry 1:1000 (#ab167453, Abcam), mouse anti-TH 1:1500 (#MAB318, Millipore), donkey anti-rabbit AlexaFluor488 and donkey anti-mouse AlexaFluor647, both 1:1000 (Jackson ImmunoResearch). For sections that were not immunostained, they were mounted with a DAPI counterstain. Images were captured with an Olympus VS120 epifluorescence microscope with a 10× objective (0.25 NA) and processed using Photoshop and Image J. The viral expression location and optic fiber placements were confirmed for all mice. Mice with off-target fiber tip placement and/or absence of viral expression were excluded from final analyses.

Acute brain slice preparation—AAV-DIO-ChR2-mCherry virus were unilaterally injected into the PVN of CRF-Cre mice. 8 weeks after the virus expression, mice were sacrificed to prepare acute brain slices for patch-clamp recordings. Briefly, mice were deeply anesthetized with a mixture of Zoletil/Xylazine (50 mg/kg / 5 mg/kg, i.p.) and perfused transcardially with ice-cold oxygenated chloride–based cutting solution containing (in mM): 93 Choline chloride, 1.2 NaH_2PO_4, 30 $NaHCO_3$, 10 $MgSO_4$, 0.5 $CaCl_2$, 2.5 KCl, 25 glucose, 3 Sodium pyruvate, 5 (+)-Sodium L-ascorbate, and 20 HEPES. Then mice were decapitated and the brain was quickly removed for blocking. Coronal brain slices containing PVN area (200-μm thickness) were prepared using a vibratome (VT1200S, Lecia, Germany) from the blocked brain tissue. The slices were recovered in artificial cerebrospinal fluid (ACSF) at 32°C for 30 min followed by incubation in ACSF at room temperature (20–24°C) for an additional 30 min before recordings. ACSF contained (in mM): 125 NaCl, 2.5 KCl, 1.3 NaH_2PO_4, 1.3 (+)-Sodium L-ascorbate, 0.6 Sodium pyruvate, 2 $CaCl_2$, 2 $MgSO_4$, 25 $NaHCO_3$, 10 glucose and was constantly bubbled with a mixture of 95% O2/5% CO_2 throughout whole experiments.

Whole-cell current-clamp recording—PVN slices were transferred to a recording chamber on a differential interference contrast (DIC) microscope stage (BX51WIF, Olympus, Japan) and were continuously perfused with oxygenated ACSF maintained at 32°C at a rate of 2–3 ml/min. PVN area was visually located using a 5x objective, as long wedge shapes on both sides adjacent to the top end of the third ventricle in the hypothalamus (interaural 3.22 mm, Bregma −0.58 mm to interaural 2.68 mm, Bregma −0.94 mm), within which neurons were identified using a 40x water immersion objective aided by fluorescence excited through a 587-nm illumination (pE-300, CoolLED, UK).

Whole-cell patch-clamp recordings were performed on the mCherry positive cells in the PVN area. Briefly, recording pipettes with resistance of 4–8 MΩ were filled with (in mM): 130 K-gluconate, 10 KCl, 10 HEPES, 1 EGTA, 2 MgATP, 0.4 NaGTP and 2 $MgCl_2$ (300 mOsm, pH adjusted to 7.2). To access responses of PVN neurons induced by optogenetic stimuli, optically-evoked APs were recorded by delivering single 470-nm optical stimuli with 10-ms or 1-s duration, and a 20Hz stimulation train (20ms on, 1-s duration), respectively. Electrophysiological signals were amplified using a Multiclamp 700B amplifier (Axon Instruments, Molecular Devices, CA). Data were low-pass filtered at 10kHz and digitized at 20 kHz using Clampex 11.1 software (Molecular Devices, CA) in conjunction with a Digidata 1550B data acquisition system (Axon Instruments, Molecular Devices, CA). Clampfit software 11.2 (Molecular Devices, CA) was used to analyze data offline. Graphs were generated in Origin 2022 (OriginLab, USA).

Methods for mDA nuclear isolation and RNA-Sequencing

Stereotaxic surgery and viral delivery.: Briefly, AAV-KASH-HA virus (AAV-pEF1a-FLEX-HA-VHH-KASH-WPRE, Addgene #129704) was injected using a 30-gauge needle and was left in place for 5 mins before retracting to ensure proper viral dispersion throughout midbrain parenchyma of Dat-Cre heterozygous mice.

Tissue dissection.: Mice were euthanized by inhalation of CO_2. Brains were quickly removed and the VTA was dissected using a scalpel. Samples were immediately frozen in liquid nitrogen and stored at −80C until processing for nuclear isolation.

Nuclear isolation.: Frozen VTA samples were homogenized in 1 mL ice-cold homogenization buffer [320 mM sucrose, 5 mM $CaCl_2$, 3 mM $Mg(Ac)_2$, 10 mM Tris pH 7.8, 0.1 mM EDTA, 0.1% NP40 (Tergitol), 1 mM β-mercaptoethanol, 0.1 mM PMSF, 1:250 RNasin Plus RNase Inhibitor (Promega), and fill to 10 mL with H2O] using a 1 mL Dounce homogenizer (Wheaton); 30 times with pestle A, followed by 30 times with pestle B. After 10 min of incubation on ice, the homogenate was filtered with a 40 μm cell strainer (Fisher), added to 1 mL of dilution buffer [50% OptiPrep density gradient medium (Sigma), 5 mM $CaCl_2$, 3 mM $Mg(Ac)_2$, 10 mM Tris pH 7.8, 1 mM β-mercaptoethanol, 0.1 mM PMSF, and fill to 1 mL with H_2O] and mixed thoroughly with a pipette. 0.5 mL of the resulting mixture was then layered on top of 0.5 mL 29% iso-osmolar OptiPrep density gradient medium solution (in PBS) in a 1.5 mL centrifugation tube and centrifuged at 6000 × g for 10 mins at 4°C. After removing the supernatant, the nuclei were resuspended in wash buffer [2.5 mM $MgCl_2$, 1% BSA in PBS, 1:250 RNasin Plus RNase Inhibitor (Promega)] for nuclear immunolabeling.

Nuclear immunolabeling.: Isolated nuclei suspended in wash buffer [2.5 mM MgCl2, 1% BSA in PBS, 1:250 RNasin Plus RNase Inhibitor (Promega)] were centrifuged (5 mins at 1000 × g) and supernatant was discarded. Nuclear pellet was resuspended with rabbit anti-HA (1:200, 3724, Cell Signaling) in 200 μL wash buffer for 1 hr and centrifuged (5 mins at 1000 × g). Supernatant was discarded and nuclear pellet was resuspended in 400 μL wash buffer for 5 mins, then centrifuged (5 mins at 1000 × g). Supernatant was removed and the nuclear pellet was then resuspended in donkey anti-rabbit 568 (1:500, A10042, Invitrogen) in 200 μL wash buffer for 1 hr, and centrifuged (5 mins at 1000 × g). Supernatant was discarded and pellet was resuspended in 400 μL wash buffer for 5 mins, and centrifuged (5 mins at 1000 × g). Nuclei were then resuspended with 1% DAPI in 500 μL wash buffer. All steps for nuclear immunolabeling were performed at 4C.

Fluorescence Assisted Nuclear Sorting.: Immunostained nuclei were then sorted using the FACS Aria II Fusion (BD) at the University of Miami Flow Cytometry Core. Nuclei were sorted based on a live-dead stain (DAPI+ vs DAPI−) and on the presence of the nuclear bound HA-tag. All intact nuclei were collected and sorted directly into 350 μL RLT Plus buffer (Qiagen) based on the presence and/or absence of the HA-tag.

RNA-Sequencing.: Total RNA from 500–1000 nuclei was extracted and normalized for input. RNAs were reverse transcribed and amplified using NEB Next Single Cell/Low Input RNA Library Prep Kit for Illumina (New England Biolabs). cDNAs were then enzymatically fragmented following manufacturer's recommendation (New England Biolabs). The fragmented cDNAs were end-repaired, adaptor ligated, and amplified using manufacturer's recommendations (New England Biolabs). Single-end 100 bp sequencing was performed by the Sylvester Comprehensive Cancer Center Oncogenomics Core (University of Miami) on a NextSeq5000 sequencer (Illumina).

RNA-Seq analysis.: All RNA-Seq data used in this study (produced by our lab or from public datasets), were mapped to the mm10 genome. Prior to mapping, raw RNA-Seq datasets were first trimmed using Trim Galore (v.0.6.6). Illumina sequence adaptors were removed, after automatic detection of the first 12–13bp. Next, reads with a length of at least 20-bp were mapped to the genome using STAR (v.2.7.8a) with the following parameters: –outSAMtype BAM SortedByCoordinate –outSAMunmapped Within –outFilterType BySJout –outSAMattributes NH HI AS NM MD XS –outFilterMultimapNmax 20 –outFilterMismatchNoverLmax 0.3 --quantMode TranscriptomeSAM GeneCounts. The resulting bam files were then passed to StringTie (v.2.1.5) to assemble sequenced alignments into estimated transcript and gene count abundance given the Gencode GRCm39 (v.M22) transcriptome assembly.

Differential gene expression analysis.: The R/Bioconductor DESeq2 package was used for differential gene expression of HA+ and HA− nuclei. Only genes with transcript abundance > 10 across samples, showing more than a two-fold expression change and a q-value < 0.05 were considered as differentially expressed.

QUANTIFICATION AND STATISTICAL ANALYSIS

The statistical details (e.g., statistical tests used, exact value of n for each experiment) can be found in the figure legends. Statistical significance was set at *p < 0.05; **p < 0.01; ***p < 0.001, ****p < 0.0001. Data are presented as means ± SEM. We analyzed all data using Prism 8 (Graphpad Software).

Supplementary Material

Refer to Web version on PubMed Central for supplementary material.

Acknowledgments

We thank Professor Erwin Neher (Max Planck Institute for Biophysical Chemistry, Göttingen, Germany), Anthony G. Phillips (University of British Columbia, Vancouver, Canada) and Ming-Hu Han (Icahn School of Medicine at Mount Sinai/Shenzhen Institutes of Advanced Technology) for their discussions and suggestions on the manuscript. We thank Professor Hongxing Zhang, Jiangning Zhou and Ji Liu for providing materials for this study. This work was supported by grants from the Science and Technology Innovation 2030 (STI2030)-Major Projects (2022ZD0207100 to ZC), the National Natural Science Foundation of China (NSFC) (31900728 to X.A.L, 32000710 to ZC, U20A2016 to ZC and TZ), the Guangdong Basic and Applied Basic Research Foundation (2019A1515110190 to ZC, 2023A1515011743 to X.A.L), Shenzhen Key Basic Research Project (JCYJ20200109115641762 to ZC), Shenzhen governmental grant (ZDSYS20190902093601675 to ZC), Science and Technology Program of Guangzhou (202102080214 to CC). and the National Institutes of Health (K01DA045294 and DP1DA051828 to LMT).

Inclusion and diversity

We support inclusive, diverse, and equitable conduct of research.

References

1. Korte SM, Koolhaas JM, Wingfield JC, and McEwen BS (2005). The Darwinian concept of stress: benefits of allostasis and costs of allostatic load and the trade-offs in health and disease. Neurosci Biobehav Rev 29, 3–38. 10.1016/j.neubiorev.2004.08.009. [PubMed: 15652252]

2. McEwen BS, and Akil H (2020). Revisiting the Stress Concept: Implications for Affective Disorders. J Neurosci 40, 12–21. 10.1523/JNEUROSCI.0733-19.2019. [PubMed: 31896560]

3. Robinson DW (1985). Stress Seeking: Selected Behavioral Characteristics of Elite Rock Climbers. Journal of Sport Psychology 7, 400–404. 10.1123/jsp.7.4.400.

4. Hollon NG, Burgeno LM, and Phillips PE (2015). Stress effects on the neural substrates of motivated behavior. Nat Neurosci 18, 1405–1412. 10.1038/nn.4114. [PubMed: 26404715]

5. Hooks MS, Juncos JL, Justice JB Jr., Meiergerd SM, Povlock SL, Schenk JO, and Kalivas PW (1994). Individual locomotor response to novelty predicts selective alterations in D1 and D2 receptors and mRNAs. J Neurosci 14, 6144–6152. 10.1523/JNEUROSCI.14-10-06144.1994. [PubMed: 7931568]

6. Kabbaj M, Devine DP, Savage VR, and Akil H (2000). Neurobiological correlates of individual differences in novelty-seeking behavior in the rat: differential expression of stress-related molecules. J Neurosci 20, 6983–6988. 10.1523/JNEUROSCI.20-18-06983.2000. [PubMed: 10995843]

7. Wand GS, Oswald LM, McCaul ME, Wong DF, Johnson E, Zhou Y, Kuwabara H, and Kumar A (2007). Association of amphetamine-induced striatal dopamine release and cortisol responses to psychological stress. Neuropsychopharmacology 32, 2310–2320. 10.1038/sj.npp.1301373. [PubMed: 17342167]

8. Tidey JW, and Miczek KA (1996). Social defeat stress selectively alters mesocorticolimbic dopamine release: an in vivo microdialysis study. Brain Res 721, 140–149. 10.1016/0006-8993(96)00159-x. [PubMed: 8793094]

9. Imperato A, Puglisi-Allegra S, Casolini P, and Angelucci L (1991). Changes in brain dopamine and acetylcholine release during and following stress are independent of the pituitary-adrenocortical axis. Brain Res 538, 111–117. 10.1016/0006-8993(91)90384-8. [PubMed: 2018923]

10. Vale W, Spiess J, Rivier C, and Rivier J (1981). Characterization of a 41-residue ovine hypothalamic peptide that stimulates secretion of corticotropin and beta-endorphin. Science 213, 1394–1397. 10.1126/science.6267699. [PubMed: 6267699]

11. Kelly EA, and Fudge JL (2018). The neuroanatomic complexity of the CRF and DA systems and their interface: What we still don't know. Neurosci Biobehav Rev 90, 247–259. 10.1016/j.neubiorev.2018.04.014. [PubMed: 29704516]

12. Kim J, Lee S, Fang YY, Shin A, Park S, Hashikawa K, Bhat S, Kim D, Sohn JW, Lin D, and Suh GSB (2019). Rapid, biphasic CRF neuronal responses encode positive and negative valence. Nat Neurosci 22, 576–585. 10.1038/s41593-019-0342-2. [PubMed: 30833699]

13. Koob GF, and Schulkin J (2019). Addiction and stress: An allostatic view. Neurosci Biobehav Rev 106, 245–262. 10.1016/j.neubiorev.2018.09.008. [PubMed: 30227143]

14. Lemos JC, and Alvarez VA (2020). The upside of stress: a mechanism for the positive motivational role of corticotropin releasing factor. Neuropsychopharmacology 45, 219–220. 10.1038/s41386-019-0510-9. [PubMed: 31511617]

15. Lemos JC, Wanat MJ, Smith JS, Reyes BA, Hollon NG, Van Bockstaele EJ, Chavkin C, and Phillips PE (2012). Severe stress switches CRF action in the nucleus accumbens from appetitive to aversive. Nature 490, 402–406. 10.1038/nature11436. [PubMed: 22992525]

16. Baumgartner HM, Schulkin J, and Berridge KC (2021). Activating Corticotropin-Releasing Factor Systems in the Nucleus Accumbens, Amygdala, and Bed Nucleus of Stria Terminalis: Incentive Motivation or Aversive Motivation? Biol Psychiatry 89, 1162–1175. 10.1016/j.biopsych.2021.01.007. [PubMed: 33726937]

17. Rasiah NP, Loewen SP, and Bains JS (2022). Windows into stress: A glimpse at emerging roles for CRH(PVN) neurons. Physiol Rev. 10.1152/physrev.00056.2021.

18. Piazza PV, Deroche V, Deminiere JM, Maccari S, Le Moal M, and Simon H (1993). Corticosterone in the range of stress-induced levels possesses reinforcing properties: implications for sensation-seeking behaviors. Proc Natl Acad Sci U S A 90, 11738–11742. 10.1073/pnas.90.24.11738. [PubMed: 8265619]

19. Yuan Y, Wu W, Chen M, Cai F, Fan C, Shen W, Sun W, and Hu J (2019). Reward Inhibits Paraventricular CRH Neurons to Relieve Stress. Curr Biol 29, 1243–1251 e1244. 10.1016/j.cub.2019.02.048. [PubMed: 30853436]

20. Cathomas F, and Russo SJ (2020). Brain-spleen connection aids antibody production. Nature 581, 142–143. 10.1038/d41586-020-01168-0. [PubMed: 32350424]
21. Zhang X, Lei B, Yuan Y, Zhang L, Hu L, Jin S, Kang B, Liao X, Sun W, Xu F, et al. (2020). Brain control of humoral immune responses amenable to behavioural modulation. Nature 581, 204–208. 10.1038/s41586-020-2235-7. [PubMed: 32405000]
22. Wanat MJ, Hopf FW, Stuber GD, Phillips PE, and Bonci A (2008). Corticotropin-releasing factor increases mouse ventral tegmental area dopamine neuron firing through a protein kinase C-dependent enhancement of Ih. J Physiol 586, 2157–2170. 10.1113/jphysiol.2007.150078. [PubMed: 18308824]
23. Wang B, Shaham Y, Zitzman D, Azari S, Wise RA, and You ZB (2005). Cocaine experience establishes control of midbrain glutamate and dopamine by corticotropin-releasing factor: a role in stress-induced relapse to drug seeking. J Neurosci 25, 5389–5396. 10.1523/JNEUROSCI.0955-05.2005. [PubMed: 15930388]
24. Stuber GD, Sparta DR, Stamatakis AM, van Leeuwen WA, Hardjoprajitno JE, Cho S, Tye KM, Kempadoo KA, Zhang F, Deisseroth K, and Bonci A (2011). Excitatory transmission from the amygdala to nucleus accumbens facilitates reward seeking. Nature 475, 377–380. 10.1038/nature10194. [PubMed: 21716290]
25. Wamsteeker Cusulin JI, Fuzesi T, Watts AG, and Bains JS (2013). Characterization of corticotropin-releasing hormone neurons in the paraventricular nucleus of the hypothalamus of Crh-IRES-Cre mutant mice. PLoS One 8, e64943. 10.1371/journal.pone.0064943. [PubMed: 23724107]
26. Kim JS, Han SY, and Iremonger KJ (2019). Stress experience and hormone feedback tune distinct components of hypothalamic CRH neuron activity. Nat Commun 10, 5696. 10.1038/s41467-019-13639-8. [PubMed: 31836701]
27. Fuzesi T, Daviu N, Wamsteeker Cusulin JI, Bonin RP, and Bains JS (2016). Hypothalamic CRH neurons orchestrate complex behaviours after stress. Nat Commun 7, 11937. 10.1038/ncomms11937. [PubMed: 27306314]
28. Taniguchi H, He M, Wu P, Kim S, Paik R, Sugino K, Kvitsiani D, Fu Y, Lu J, Lin Y, et al. (2011). A resource of Cre driver lines for genetic targeting of GABAergic neurons in cerebral cortex. Neuron 71, 995–1013. 10.1016/j.neuron.2011.07.026. [PubMed: 21943598]
29. Zell V, Steinkellner T, Hollon NG, Warlow SM, Souter E, Faget L, Hunker AC, Jin X, Zweifel LS, and Hnasko TS (2020). VTA Glutamate Neuron Activity Drives Positive Reinforcement Absent Dopamine Co-release. Neuron 107, 864–873 e864. 10.1016/j.neuron.2020.06.011. [PubMed: 32610039]
30. Volkow ND, Wise RA, and Baler R (2017). The dopamine motive system: implications for drug and food addiction. Nat Rev Neurosci 18, 741–752. 10.1038/nrn.2017.130. [PubMed: 29142296]
31. Witten IB, Steinberg EE, Lee SY, Davidson TJ, Zalocusky KA, Brodsky M, Yizhar O, Cho SL, Gong S, Ramakrishnan C, et al. (2011). Recombinase-driver rat lines: tools, techniques, and optogenetic application to dopamine-mediated reinforcement. Neuron 72, 721–733. 10.1016/j.neuron.2011.10.028. [PubMed: 22153370]
32. Denver RJ (2009). Structural and functional evolution of vertebrate neuroendocrine stress systems. Ann N Y Acad Sci 1163, 1–16. 10.1111/j.1749-6632.2009.04433.x. [PubMed: 19456324]
33. Totani Y, Niinomi M, Takatsuki K, Oiso Y, and Tomita A (1990). Effect of metyrapone pretreatment on adrenocorticotropin secretion induced by corticotropin-releasing hormone in normal subjects and patients with Cushing's disease. J Clin Endocrinol Metab 70, 798–803. 10.1210/jcem-70-3-798. [PubMed: 2155255]
34. Hung LW, Neuner S, Polepalli JS, Beier KT, Wright M, Walsh JJ, Lewis EM, Luo L, Deisseroth K, Dolen G, and Malenka RC (2017). Gating of social reward by oxytocin in the ventral tegmental area. Science 357, 1406–1411. 10.1126/science.aan4994. [PubMed: 28963257]
35. Steinberg EE, Boivin JR, Saunders BT, Witten IB, Deisseroth K, and Janak PH (2014). Positive reinforcement mediated by midbrain dopamine neurons requires D1 and D2 receptor activation in the nucleus accumbens. PLoS One 9, e94771. 10.1371/journal.pone.0094771. [PubMed: 24733061]

36. Tuesta LM, Djekidel MN, Chen R, Lu F, Wang W, Sabatini BL, and Zhang Y (2019). In vivo nuclear capture and molecular profiling identifies Gmeb1 as a transcriptional regulator essential for dopamine neuron function. Nat Commun 10, 2508. 10.1038/s41467-019-10267-0. [PubMed: 31175277]
37. Garris PA, Kilpatrick M, Bunin MA, Michael D, Walker QD, and Wightman RM (1999). Dissociation of dopamine release in the nucleus accumbens from intracranial self-stimulation. Nature 398, 67–69. 10.1038/18019. [PubMed: 10078530]
38. Sun F, Zhou J, Dai B, Qian T, Zeng J, Li X, Zhuo Y, Zhang Y, Wang Y, Qian C, et al. (2020). Next-generation GRAB sensors for monitoring dopaminergic activity in vivo. Nat Methods 17, 1156–1166. 10.1038/s41592-020-00981-9. [PubMed: 33087905]
39. Green TA, and Bardo MT (2020). Opposite regulation of conditioned place preference and intravenous drug self-administration in rodent models: Motivational and non-motivational examples. Neurosci Biobehav Rev 116, 89–98. 10.1016/j.neubiorev.2020.06.006. [PubMed: 32534899]
40. Hunt AJ Jr., Dasgupta R, Rajamanickam S, Jiang Z, Beierlein M, Chan CS, and Justice NJ (2018). Paraventricular hypothalamic and amygdalar CRF neurons synapse in the external globus pallidus. Brain Struct Funct 223, 2685–2698. 10.1007/s00429-018-1652-y. [PubMed: 29569009]
41. Wanat MJ, Bonci A, and Phillips PE (2013). CRF acts in the midbrain to attenuate accumbens dopamine release to rewards but not their predictors. Nat Neurosci 16, 383–385. 10.1038/nn.3335. [PubMed: 23416448]
42. Tunstall BJ, and Carmack SA (2016). Social Stress-Induced Alterations in CRF Signaling in the VTA Facilitate the Emergence of Addiction-like Behavior. J Neurosci 36, 8780–8782. 10.1523/JNEUROSCI.1815-16.2016. [PubMed: 27559161]
43. Holly EN, Boyson CO, Montagud-Romero S, Stein DJ, Gobrogge KL, DeBold JF, and Miczek KA (2016). Episodic Social Stress-Escalated Cocaine Self-Administration: Role of Phasic and Tonic Corticotropin Releasing Factor in the Anterior and Posterior Ventral Tegmental Area. J Neurosci 36, 4093–4105. 10.1523/JNEUROSCI.2232-15.2016. [PubMed: 27053215]
44. Zalachoras I, Astori S, Meijer M, Grosse J, Zanoletti O, de Suduiraut IG, Deussing JM, and Sandi C (2022). Opposite effects of stress on effortful motivation in high and low anxiety are mediated by CRHR1 in the VTA. Sci Adv 8, eabj9019. 10.1126/sciadv.abj9019. [PubMed: 35319997]
45. Hupalo S, Bryce CA, Bangasser DA, Berridge CW, Valentino RJ, and Floresco SB (2019). Corticotropin-Releasing Factor (CRF) circuit modulation of cognition and motivation. Neurosci Biobehav Rev 103, 50–59. 10.1016/j.neubiorev.2019.06.010. [PubMed: 31212019]
46. Jiang C, Yang X, He G, Wang F, Wang Z, Xu W, Mao Y, Ma L, and Wang F (2021). CRH(CeA-->VTA) inputs inhibit the positive ensembles to induce negative effect of opiate withdrawal. Mol Psychiatry 26, 6170–6186. 10.1038/s41380-021-01321-9. [PubMed: 34642456]
47. Henckens MJ, Deussing JM, and Chen A (2016). Region-specific roles of the corticotropin-releasing factor-urocortin system in stress. Nat Rev Neurosci 17, 636–651. 10.1038/nrn.2016.94. [PubMed: 27586075]
48. Ungless MA, Singh V, Crowder TL, Yaka R, Ron D, and Bonci A (2003). Corticotropin-releasing factor requires CRF binding protein to potentiate NMDA receptors via CRF receptor 2 in dopamine neurons. Neuron 39, 401–407. 10.1016/s0896-6273(03)00461-6. [PubMed: 12895416]
49. Borgland SL, Ungless MA, and Bonci A (2010). Convergent actions of orexin/hypocretin and CRF on dopamine neurons: Emerging players in addiction. Brain Res 1314, 139–144. 10.1016/j.brainres.2009.10.068. [PubMed: 19891960]
50. Lovenberg TW, Liaw CW, Grigoriadis DE, Clevenger W, Chalmers DT, De Souza EB, and Oltersdorf T (1995). Cloning and characterization of a functionally distinct corticotropin-releasing factor receptor subtype from rat brain. Proc Natl Acad Sci U S A 92, 836–840. 10.1073/pnas.92.3.836. [PubMed: 7846062]
51. Ulrich-Lai YM, and Herman JP (2009). Neural regulation of endocrine and autonomic stress responses. Nat Rev Neurosci 10, 397–409. 10.1038/nrn2647. [PubMed: 19469025]
52. Anderson SM, Bari AA, and Pierce RC (2003). Administration of the D1-like dopamine receptor antagonist SCH-23390 into the medial nucleus accumbens shell attenuates cocaine priming-

induced reinstatement of drug-seeking behavior in rats. Psychopharmacology (Berl) 168, 132–138. 10.1007/s00213-002-1298-5. [PubMed: 12491029]

53. Young EA, Dreumont SE, and Cunningham CL (2014). Role of nucleus accumbens dopamine receptor subtypes in the learning and expression of alcohol-seeking behavior. Neurobiol Learn Mem 108, 28–37. 10.1016/j.nlm.2013.05.004. [PubMed: 23742917]
54. Wook Koo J, Labonte B, Engmann O, Calipari ES, Juarez B, Lorsch Z, Walsh JJ, Friedman AK, Yorgason JT, Han MH, and Nestler EJ (2016). Essential Role of Mesolimbic Brain-Derived Neurotrophic Factor in Chronic Social Stress-Induced Depressive Behaviors. Biol Psychiatry 80, 469–478. 10.1016/j.biopsych.2015.12.009. [PubMed: 26858215]

Highlights:

- Activation of the PVN^{CRF} neurons or their fibers in VTA supports self-stimulation
- The self-stimulation behaviors are not mediated by the activation of the HPA axis
- Stimulation of PVN^{CRF}→VTA circuitry enhances VTA-derived DA release in the NAc
- The reinforcing effect of PVN^{CRF}→VTA circuitry requires DA transmission in the NAc

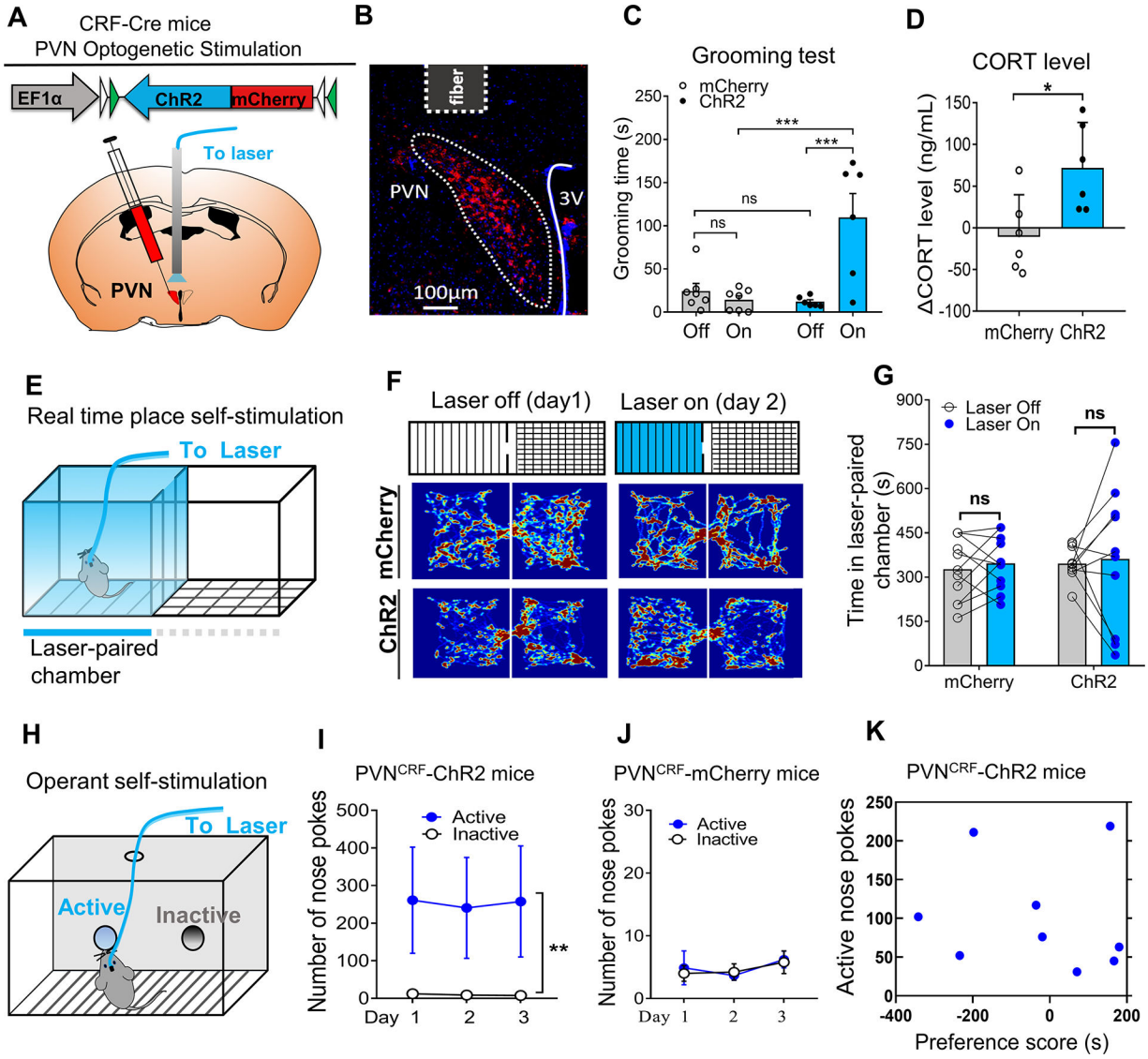

Figure 1. Selective activation of PVN CRF cell bodies promotes operant self-stimulation behaviors.

(A) Schematic map of the strategy for selective activation of PVN CRF neurons. A fiber was implanted above PVN for optical stimulation. (B) Image shows the expression of the ChR2 virus in the PVN. Scale bar, 100 μm. (C) Optical stimulation markedly increased the grooming time in the PVN^{CRF}-ChR2 mice, but not in the control mice. ChR2 mice, n = 6; mCherry mice, n = 7; ***p < 0.001, Two-way ANOVA, Bonferroni post hoc test. (D) Optical stimulation significantly increased plasma corticosterone levels in the PVN^{CRF}-ChR2 mice compared with those in the control mice (n = 6 in both groups; unpaired t-test, *p < 0.05). (E) Depiction of the place self-stimulation for RTPP/A behaviors paradigm in an apparatus with two-connected chambers. One of the chambers was paired with laser stimulation, entrance into this chamber immediately turned on the laser and continuously on until the animal exited. (F) Representative locomotor traces during baseline (laser off) and RTPP/A (laser on) tests from one animal in each group. (G) Summary for the time of each individual mouse spent in the laser-paired chamber during baseline and RTPP/A tests

(mCherry, n=11, Laser off vs Laser on: p = 0.9; ChR2, n=10, Laser off vs Laser on: p =0.9; ns, no significant, Two-way ANOVA, Bonferroni post hoc test). (H) Depiction of the optogenetic self-stimulation behaviors paradigm in an operant chamber. Animal was trained to nose poke into an active port to receive optical stimulation; nose poke into an inactive port would not trigger optical stimulation. (I) The PVN^{CRF}-ChR2 mice had stable and robust active port responses over three consecutive daily sessions (30 min for each session) (n =8 mice; Two-way repeated measures (RM-ANOVA), active nose pokes vs. inactive nose pokes, $F(1,14) = 8.5$, $^{**}p < 0.01$). (J) The control mice had low responses at both active and inactive port (n = 8 mice; Two-way RM-ANOVA, active nose pokes vs. inactive nose pokes, $F(1, 14) = 0.5$, $p = 0.8$). (K) The active nose pokes number was plotted with the preference score for each individual animal in the ChR2 group shown in G. The preference score was calculated as the time spent in the laser paired chamber during RTPP/A test minus those during baseline test. Note that the 3 mice shown strong avoidance in RTPP/A test also responded at high levels at active ports. There was no significant correlation between active nose pokes number and preference score. $R=0.15$, $p=0.75$. Data are presented as mean ± S.E.M. See also Figures S1–S3 and Videos S1–S2.

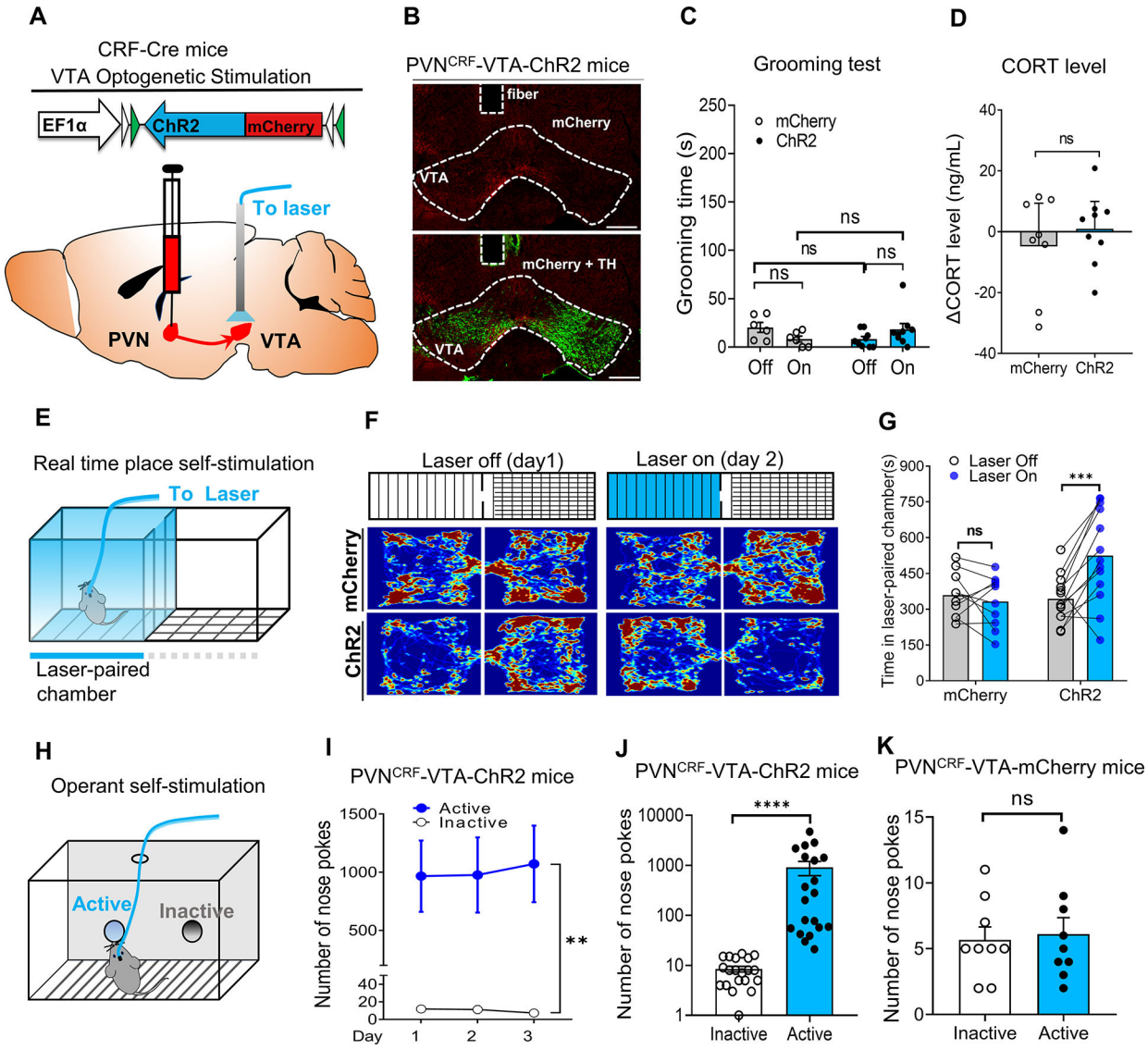

Figure 2. Selective activation of PVN CRF neuronal projections to VTA promotes reward-related behaviors.

(A) Schematic map for strategy of selective activation of PVN CRF neuronal projections to VTA. A fiber was implanted above VTA for optical stimulation. (B) Images showing the expression of ChR2-mCherry in the VTA which was highlighted with TH positive cells. Scale bar, 300 μm. (C) Optical stimulation didn't affect grooming behaviors in either PVN^{CRF}-VTA-ChR2 mice (n = 9) or their control mice (n = 6). Two-way RM ANOVA; Laser off vs Laser on, F (1, 14) = 0.33, p = 0.57; mCherry vs ChR2, F (1, 14) = 0.4161, p = 0.53. (D) Optical stimulation didn't change the plasma CORT levels in either PVN^{CRF}-VTA-ChR2 mice (n = 9) or the control mice (n = 8). Unpaired t test, p = 0.45. (E) Depiction of the place self-stimulation for RTPP/A behavior paradigm in an apparatus with two-connected chambers. (F-G) Optical stimulation induced real time place preference in the PVN^{CRF}-VTA-ChR2, but not in the control mice. The representative locomotor traces were shown in F. The time spent in the laser-paired chamber during baseline and RTPP/A tests

from each individual animal was summarized in G. mCherry, n = 10, Laser off vs Laser on:, p = 0.79; ChR2, n=13, Laser off vs Laser on: ***p<0.001; Two-way ANOVA, Bonferroni post hoc test.). (H) Depiction of the optogenetic self-stimulation behavior paradigm in an operant chamber. (I)The PVN^{CRF}-VTA-ChR2 mice had stable and high active port responses over 3 consecutive daily sessions (30 mins for each section) (n = 12 mice; Two-way RM-ANOVA, number of active nose pokes vs inactive nose pokes, F (1, 22) = 9.5, **p < 0.01; day effect, F(2, 44), p = 0.476). (J, K) Average number of inactive and active nose pokes during a 30-min operant self-stimulation section from PVN^{CRF}-VTA-ChR2 (J) and the control mice (K). The PVN^{CRF}-VTA-ChR2 mice had much higher active nose pokes than inactive nose pokes, but not the control mice. ChR2 group, n = 20 mice; Mann Whitney test, ****p < 0.0001. mCherry group, n=9; active nose poke vs; unpaired t test, p = 0.78. Data are presented as mean ± S.E.M. See also Figures S4–S5 and Video S3.

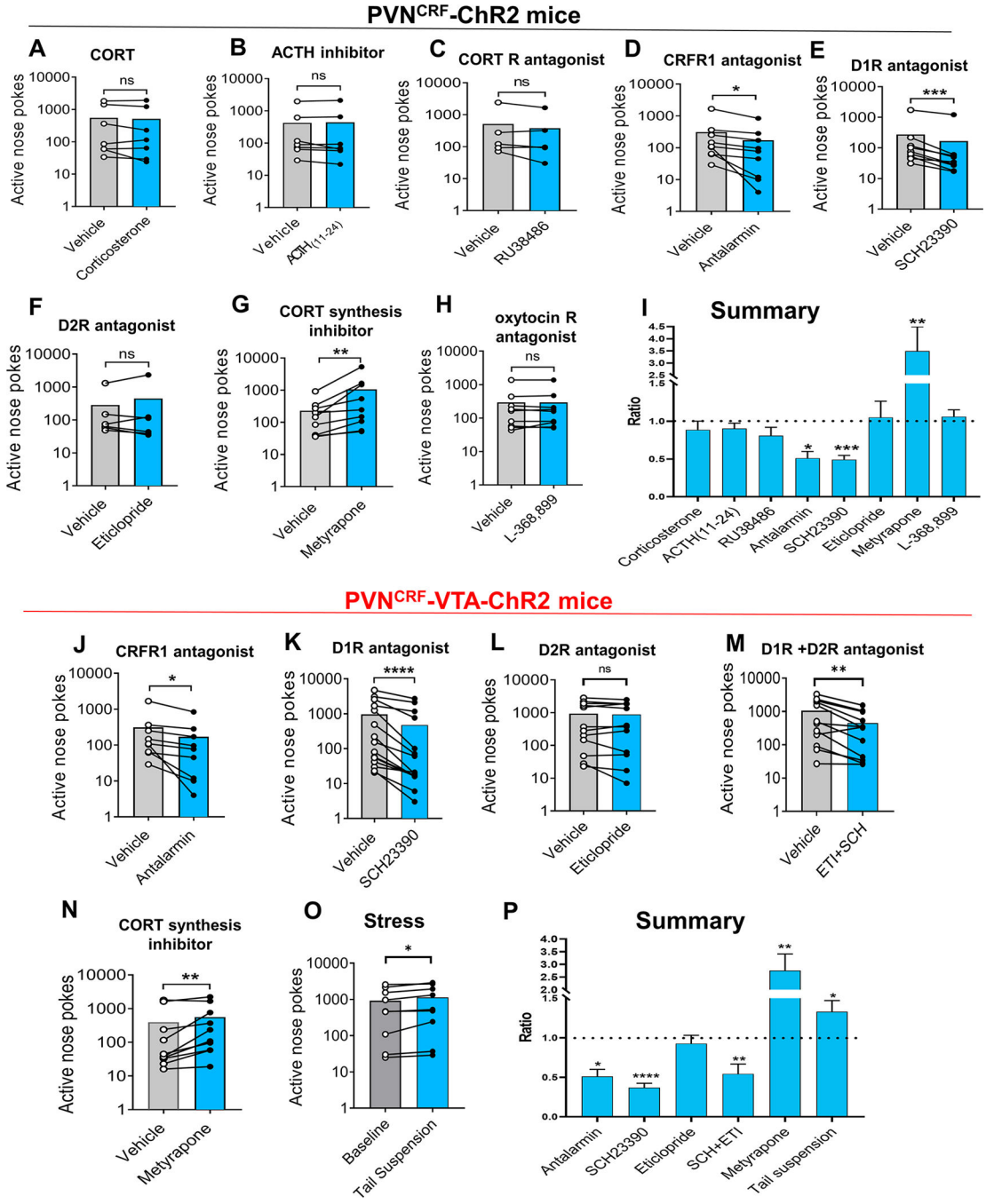

Figure 3. Manipulations of the operant self-stimulation behaviors in PVN^{CRF}-ChR2 and PVN^{CRF}-VTA-ChR2 mice, respectively.

(A-I) Manipulations of the operant self-stimulation behaviors in the PVN^{CRF}-ChR2 mice with pharmacological tools via systemic injections. (A) Corticosterone (n = 7 mice; p = 0.27); (B) ACTH$_{(11–24)}$ (n = 7 mice; p = 0.22); (C) RU38486 (n = 6 mice; p = 0.14); (D) Antalarmin (n= 9 mice; *p < 0.05); (E) SCH23390 (n = 9 mice, ***p < 0.001); (F) Eticlopride (n = 6 mice; p = 0.82); (G) Metyrapone (n = 9 mice; **p < 0.01); (H) L-368,899 (n = 9 mice; p = 0.61); (I) Summary for the effects of pretreatment in the PVN^{CRF}-ChR2 mice. (J-O) Manipulations of the operant self-stimulation behaviors in the PVN^{CRF}-VTA-

ChR2 mice with pharmacological tools via systemic injection or with acute stress. (J) Antalarmin (n = 9 mice; *p < 0.05); (K) SCH23390 (n = 15 mice, ****p < 0.0001); (L) Eticlopride (n = 12 mice, p = 0.26); (M) SCH23390 + Eticlopride (n = 12, **p < 0.01); (N) Metyrapone (n = 9 mice; **p < 0.01); (O) 2-min tail suspension induced stress (n = 11 mice, *p < 0.05); (P) Summary for the effects of pretreatments in the PVN^{CRF}-VTA-ChR2 mice. The ratio was calculated by dividing the active nosepoke number from the treatment section to the active nosepoke number from the vehicle or baseline section for each animal. Paired ratio t test was used for statistics analysis. Data are presented as mean ± S.E.M. See also Figure S6.

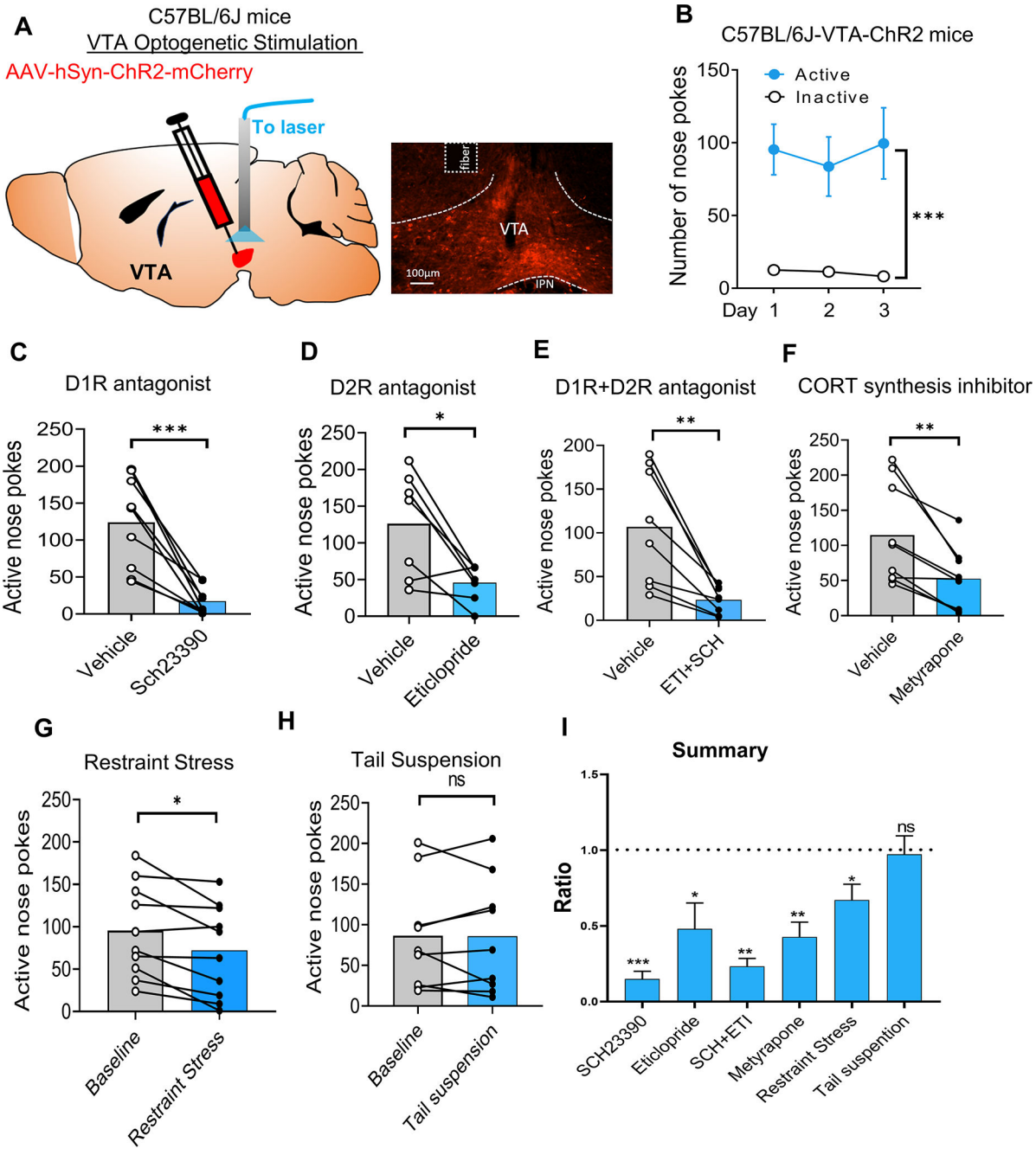

Figure 4. Operant self-stimulation behavior in the C57BL/6J-VTA-ChR2 mice.

(A) Schematic map for strategy of optogenetic activation of VTA neurons (left) and a representative image shows virus expression and fiber implantation in the VTA (right). AAV-hSyn-ChR2-mCherry virus was injected unilaterally into the VTA of C57BL/6J mice and an optic fiber was implanted above the injection site for optical stimulation. (B) The C57BL/6J-VTA-ChR2 mice had stable and robust active nose pokes over 3 consecutive daily sessions (30 mins for each section) (n = 10 mice; Two-way RM-ANOVA, number of active nose-pokes vs inactive nose-pokes, F (1, 18) = 18.26, ***p < 0.001; day effect, F(2, 30), p = 0.5749). (C-I) The number of active nose pokes for self-stimulation was assessed

with pretreatment of individual drugs and vehicles (i.p injection), or with acute stress. (C) SCH23390 (n = 9 mice, ***p < 0.0001); (D) Eticlopride (n = 7 mice, *p < 0.05; (E) SCH23390 + Eticlopride (n = 8, **p < 0.01); (F) Metyrapone (n = 9 mice; **p < 0.01); (G) 10-min restraint stress (n = 10 mice, *p < 0.05); (H) 2-min tail suspension induced stress (n = 9 mice, p = 0.93); (I) Summary of the effects of pretreatment in C-H. Paired ratio t test was used for statistics analyses. Data are presented as mean ± S.E.M.

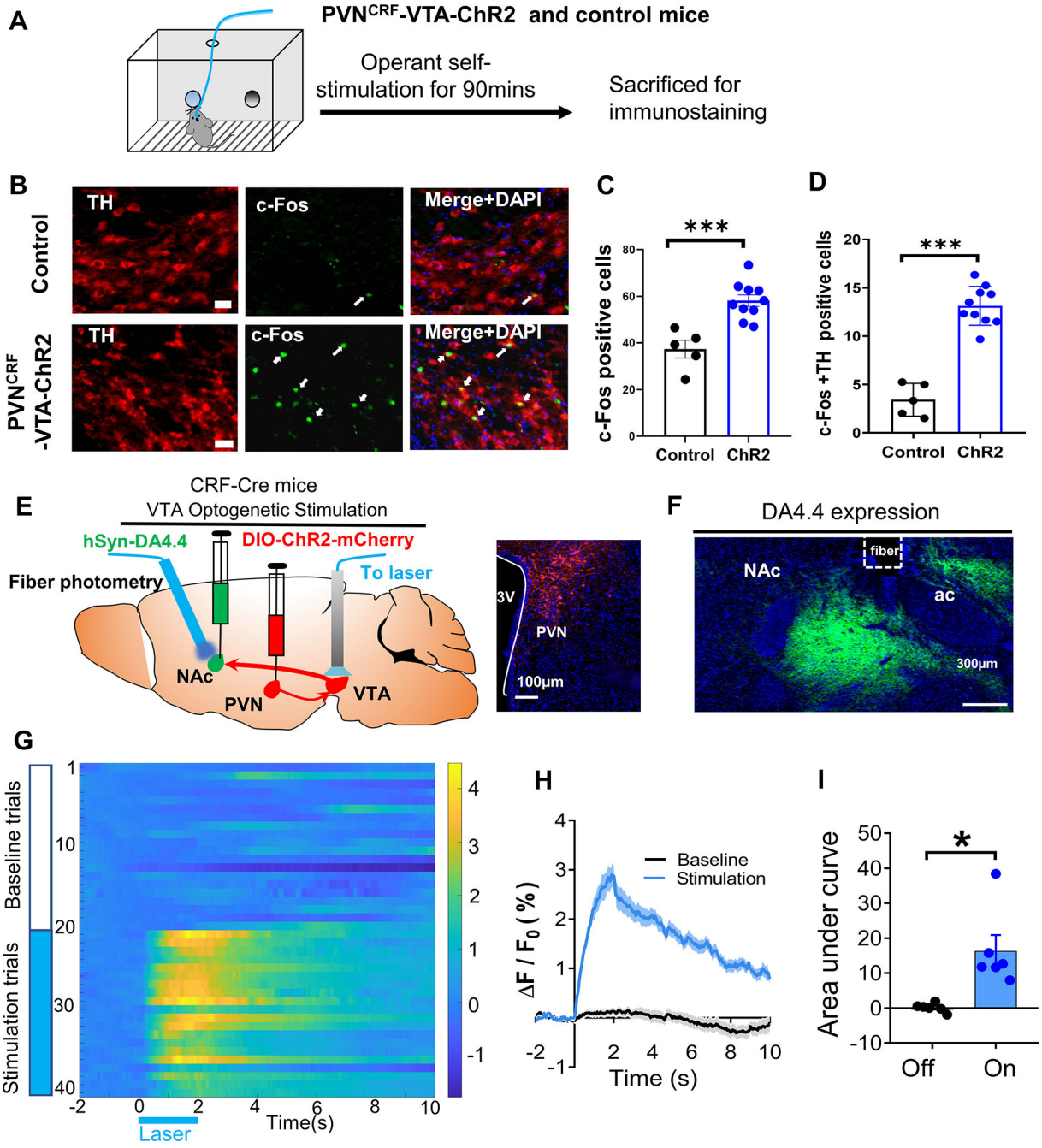

Figure 5. Activation of PVN CRF projections increases neural activity of TH+ cells in VTA and induces VTA-deprived dopamine release in NAc.

(A-D) Operant self-stimulation increased c-Fos expression in VTA of PVN^{CRF}-VTA-ChR2 mice. (A) Experiment procedure. (B) Representative images for TH and c-Fos immunostaining on VTA brain slices from control mice and PVN^{CRF}-VTA-ChR2 mice, respectively. Scale bar, 20 μm. (C) Bargraph showing the average number of c-Fos positive cells per slice in each animal. ***, $p<0.001$. (D) Bargraph showing the average number of c-Fos and TH double-positive cells per slice in each animal. ****, $p<0.0001$. 3–5 brain slices for each animal were analyzed. (E-I) In vivo photometry recording dopamine sensor

signal in NAc while stimulating the PVN CRF projections to VTA. (E) Schematic map for strategy of activation of PVN CRF projections to VTA and monitoring in vivo dopamine release at NAc (left). A representative image shows the ChR2-mCherry expression in the PVN (right). (F) Representative image showing the expression of dopamine sensor $DA_{4.4}$ in the NAc. Scale bar, 300 μm. (G) Representative heatmap of $DA_{4.4}$ fluorescence in the NAc in response to terminal stimulation in the VTA from one mouse. 20 trials were performed with the laser-off to get the baseline, followed by 20 trials with the laser-on stimulation. At each trial, stimulation started at 0 s and ended at 2 s. (H, I) Average of fluorescence traces ($\Delta F/F0$) of $DA_{4.4}$ at the baseline and that in response to the optogenetic stimulations (H) and the area under the curve (I) ($n = 6$ mice; paired t test, $^*p < 0.05$). Data are presented as mean ± S.E.M.

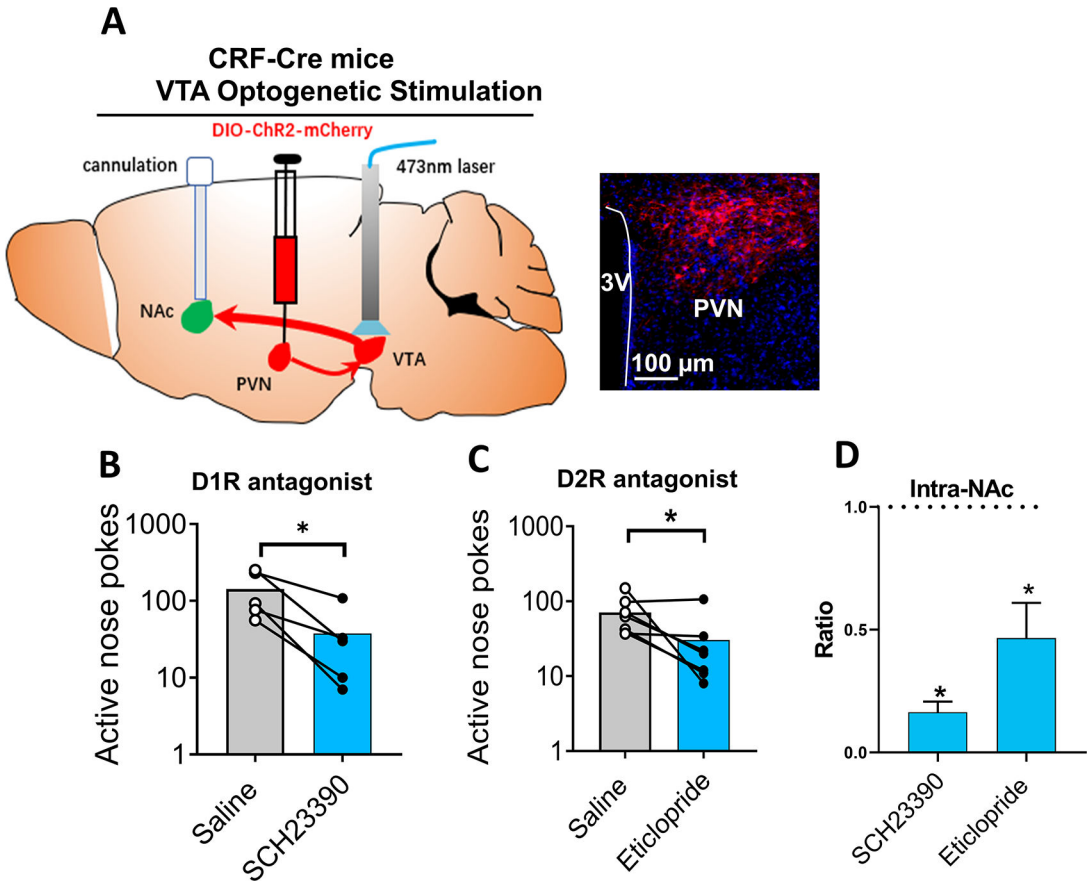

Figure 6. The positive reinforcing effect of PVN^{CRF}→VTA projections requires activation of D1R and D2R in the NAc.

(A) Schematic map for self-stimulation of PVN^{CRF}→VTA projections with drug infusions intoNAc (left). A representative image shows the ChR2-mCherry expression in the PVN (right). (B-C) Micro-infusion of D1R antagonist SCH23390 (B) or D2R antagonist Eticlopride (C) significantly attenuated the self-stimulation behaviors of PVN^{CRF}→VTA projections. SCH23390 (n = 5 mice, *$p < 0.01$); Eticlopride (n=7 mice, *$p < 0.01$). (D) Summary of the effects of pretreatments in *B-C*. Paired ratio *t* test was used for statistics analyses. Data are presented as mean ± S.E.M.

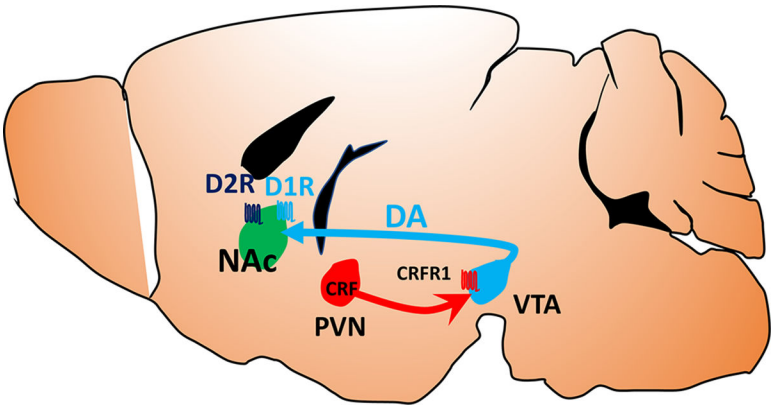

Figure 7. A working hypothesis for the positive rewarding effect of PVN CRF neurons.

Activation of the PVN CRF neurons results in CRF release in the VTA, which excites the CRFR1-expressing DA neurons and then induces dopamine transmission in the D1R and D2R-expressing neurons in the NAc. See also Figure S6.

KEY RESOURCES TABLE

REAGENT or RESOURCE	SOURCE	IDENTIFIER
Antibodies		
mCherry antibody	Abcam	Cat# ab167453
TH antibody	Millipore	Cat# MAB318
c-Fos antibody	Cell Signaling	Cat# 2250S
HA-Tag (C29F4) Rabbit mAb	Cell Signaling	Cat# 3724
Alexa Fluor® 488 AffiniPure Donkey Anti-Rabbit IgG (H+L)	Jackson ImmunoResearch	Cat# 711-545-152 RRID: AB_2313584
Alexa Fluor® 647 AffiniPure Donkey Anti-Mouse IgG (H+L)	Jackson ImmunoResearch	Cat# 715-605-151 RRID: AB_2340863
Donkey anti-Rabbit IgG (H+L) Highly Cross-Adsorbed Secondary Antibody, Alexa Fluor™ 568	Invitrogen	Cat# A10042
Bacterial and virus strains		
AAV2/9-hEF1α-DIO-mCherry	Shanghai Taitool Bioscience Co., Ltd., China	Cat# S0197-9
AAV2/9-hEF1α-DIO-hChR2(H134R)-mCherry	Shanghai Taitool Bioscience Co., Ltd.	Cat# S0170-9
AAV2/9-hSyn-hChR2(H134R)-mCherry	BrainVTA Co., Ltd., China	Cat# BC0097
AAV9-hSyn-DA4.4	Vigene Biosciences Co., Ltd., China	Cat# NTA-2012-ZP568
AAV-pEF1a-FLEX-HA-VHH-KASH-WPRE	Addgene	Cat# 129704
Chemicals, peptides, and recombinant proteins		
Antalarmin	Absin	Cat# abs823290
SCH23390	MedChemExpress	Cat# HY-19545A
Eticlopride	MedChemExpress	Cat# HY-03413
Corticosterone	Sigma-Aldrich	Cat# C2505
Metyrapone	Absin	Cat# abs816604
Normal Donkey Serum	Jackson ImmunoResearch	Cat# 017-000-121
Normal Goat Serum	Jackson ImmunoResearch	Cat# 005-000-121
DAPI nuclear counterstain	Vector Labs	Cat# SP-8500-15
RNasin® Ribonuclease Inhibitors	Promega	Cat# N2111
Critical commercial assays		
CORT ELISA KIT	Abcam	Cat# ab108821
NEB Next Single Cell/ Low Input RNA Library Prep Kit	New England Biolabs	Cat# E6420
Experimental models: Organisms/strains		
C57BL/6J mice	GemPharmatech	N/A
B6(Cg)-Crh$^{tm1(cre)Zjh}$/J mice	Jackson Lab	JAX: 012704
Software and algorithms		
GraphPad Prism 8	GraphPad Software	https://www.graphpad.com/scientific-software/prism/
MATLAB	The MathWorks	RRID: SCR_001622

REAGENT or RESOURCE	SOURCE	IDENTIFIER
Image J	NIH	https://imagej.nih.gov/j/
Digidata 1550B data acquisition system	Axon Instruments, Molecular Devices Co., Ltd., CA	https://www.moleculardevices.com
Clampex 11.1 software	Molecular Devices, CA	https://www.moleculardevices.com/
Other		
Stereotaxic instrument	RWD Life Science Co., Ltd., China	G1080201
Patch cables	Nanjing Aoguan Bioscience Co., Ltd., China	CFJ-1CT
Epifluorescence microscope	Olympus	VS120
Differential interference contrast microscope	Olympus Co., Ltd., Japan	BX51WIF